

AN ABSTRACT OF THE THESIS OF

Michael E. Rising for the degree of Master of Science in Nuclear Engineering presented on May 16, 2008.

Title: Analysis of the Method of Tubes Characteristic Schemes in the Thick Diffusive Limit.

Abstract approved: _____

Todd S. Palmer

Characteristic methods are widely known to be very accurate approaches to the solution of numerical transport problems. These methods are most often used for neutron transport applications (i.e. lattice physics calculations) where spatial cells are of intermediate optical thickness ($O(1)$ - $O(100)$ mean free paths, depending on the energy group) and materials are not exceptionally highly scattering (scattering ratios < 0.999). There has been interest in using characteristic methods for radiative transfer applications, which often involve very optically thick and diffusive regions. Previous work has involved analyses of families of Cartesian geometry characteristic methods in optically thick and diffusive regions. There is a significant body of work in the Russian literature on curvilinear geometry characteristic methods, but very few analyses of their behavior in thick diffusive regions have been published. This thesis will focus on the diffusion limit of a specific family of 1-D spherical geometry characteristic methods - the method of tubes (MOT). In these methods, the streaming operator is transformed via a change of coordinates into a slab-geometry-like form.

First we present two MOT discretizations published in the Russian literature and two new variants (SC, LC) based on traditional slab geometry characteristic approaches. We have performed asymptotic analyses of these four characteristic

methods and have verified these analyses with numerical results.

Optically thick and diffusive problems are often very computationally expensive to solve using the traditional “source iteration” iterative method. We have developed an efficient acceleration technique for the most promising version of the MOT (LC) based on an approach developed for the slab geometry linear discontinuous finite element method.

The LC version of the MOT that we have developed has very good thick diffusion limit behavior and many other very attractive properties.

©Copyright by Michael E. Rising

May 16, 2008

All Rights Reserved

Analysis of the Method of Tubes Characteristic Schemes in the Thick Diffusive
Limit

by

Michael E. Rising

A THESIS

submitted to

Oregon State University

in partial fulfillment of
the requirements for the
degree of

Master of Science

Presented May 16, 2008
Commencement June 2009

Master of Science thesis of Michael E. Rising presented on May 16, 2008.

APPROVED:

Major Professor, representing Nuclear Engineering

Head of the Department of Nuclear Engineering and Radiation Health Physics

Dean of the Graduate School

I understand that my thesis will become part of the permanent collection of Oregon State University libraries. My signature below authorizes release of my thesis to any reader upon request.

Michael E. Rising, Author

ACKNOWLEDGEMENTS

First and foremost, I would like to thank my advisor, Dr. Todd Palmer. I have had a great experience being a student of his as an undergraduate from 2002-2006 and as a graduate for the past two years. Dr. Palmer has always been extremely patient, thoughtful, and considerate in every interaction I have had with him. Whether in the classroom or in a research meeting, his guidance has made being a student of his an extremely rewarding experience. If I am one day regarded as even a fraction of the scientist, mentor, and friend that he is to so many people, I will be very happy.

It is also important for me to thank Dr. Palmer, Oregon State University, and the A/X Division at Lawrence Livermore National Laboratory (LLNL) for financially supporting me for the past two years.

I would like to thank the remaining members of my thesis committee, Dr. Brian Woods from the Department of Nuclear Engineering and Radiation Health Physics, Dr. Kenneth Krane from the Department of Physics, and Dr. Sourabh Apte from the Department of Mechanical Engineering.

I need to also acknowledge the help from Dr. Dmitriy Anistratov from North Carolina State University. His willingness to participate in several helpful discussions over the past couple years made completing this research possible.

I would also like to thank a few graduate students and friends that have made my experiences at both LLNL and at Oregon State University very worthwhile. In no particular order, I would like to thank Alex Misner, Matt Cleveland, Nathan Barnett, Teresa Bailey, Brian Collins, Tony Elliot, Brennan Garrelts, Burke van Patten, and Anne Foster.

Also, I would like to acknowledge the love and support provided to me by my family. My fiancée Heather has given me the strength and motivation to pursue my academic and career goals. Without her consistent support over the last several years I would likely not be where I am today. She has made my life far more worthwhile and I look forward to our long life together. I should also thank my grandfather Lou Jalbert, aunt and uncle, Carol and Carl, and cousins Kayla and Grant and various other family members too numerous to name. Although they are not directly related, I would like to thank the Lahti's and in particular Zane for our close friendship over the years.

Last, but certainly not least, I am deeply appreciative of the love and support of my mother and father, Susan and David Rising. Over the last 24 years they have assisted me in achieving all of my goals. Without their steady influence in my life and countless ways of supporting me, none of those goals would have been possible to achieve.

This research was performed under a research grant from Lawrence Livermore National Laboratory's' A/X Division.

TABLE OF CONTENTS

	<u>Page</u>
1 INTRODUCTION	1
1.1 Literature Review	2
1.1.1 Characteristic Transport Methods in Thick, Diffusive Regimes	3
1.1.2 1-D Spherical Geometry Characteristic Methods	4
1.1.3 Source Iteration and Diffusion Synthetic Acceleration	5
1.2 Thesis Overview	6
2 THE SPHERICAL GEOMETRY NEUTRAL PARTICLE TRANSPORT EQUATION	8
2.1 Introduction	8
2.2 Space-Angle Discretization	10
3 THE “METHOD OF TUBES” FAMILY OF CHARACTERISTIC METHODS	14
3.1 Introduction	14
3.2 Original Method of Tubes Schemes	17
3.2.1 Original MOT Constant (Step) Source Method (MOT-SS)	18
3.2.2 Original MOT Linear Source Method (MOT-LS)	19
3.3 Moment-Based Method of Tubes Schemes	20
3.3.1 Moment-Based Step Characteristic MOT (SCMOT)	20
3.3.2 Moment-Based Linear Characteristic MOT (LCMOT)	21
4 ASYMPTOTIC DIFFUSION ANALYSIS	23
4.1 Introduction	23
4.2 Asymptotic Analysis Procedure	25

TABLE OF CONTENTS (Continued)

	<u>Page</u>
4.2.1 Analysis of MOT-SS	25
4.2.2 Analysis of SCMOT	29
4.2.3 Analysis of LCMOT	33
5 DIFFUSION SYNTHETIC ACCELERATION OF LCMOT	41
5.1 Introduction	41
5.2 Linear Discontinuous Method of Tubes (LDMOT)	41
5.3 Modified Four-Step	44
6 RESULTS	53
6.1 Introduction	53
6.2 Test Problems	54
6.2.1 Reed Test Problem	54
6.2.2 A Test with a Diffusion Region	55
6.2.3 A Diffusion Test with an Unresolved Boundary Layer	57
6.2.4 A Set of Tests on the Asymptotic Diffusion Limit	61
7 CONCLUSIONS	66
7.1 Introduction	66
7.2 Original MOT Discretizations (MOT-SS and MOT-LS)	67
7.3 Moment-Based MOT Discretizations (SCMOT and LCMOT)	68
7.4 Diffusion Synthetic Acceleration of LCMOT	69
7.5 Overall Conclusions and Future Work	69
BIBLIOGRAPHY	71

LIST OF FIGURES

<u>Figure</u>		<u>Page</u>
1	1-D Spherical Geometry Coordinate System.	9
2	Discretized Space-Angle Grid in (r, μ) Coordinates.	11
3	Phase Space Volume Element (t, i) in (r, μ) Coordinates.	12
4	Problem 1 Solutions for all MOT Schemes and a “Fully-Lumped” LD Scheme.	55
5	Problem 2 Solutions for all MOT Schemes.	56
6	Problem 3 Solutions for all MOT Schemes.	59
7	Problem 3 Interior Solutions for all MOT Schemes.	59
8	Problem 3’ Solutions for all MOT Schemes.	60
9	Problem 3’ Interior Solutions for all MOT Schemes.	61
10	Problem 4 Solutions for the MOT-SS Scheme.	62
11	Problem 4 Solutions for the MOT-LS Scheme.	63
12	Problem 4 Solutions for the SCMOT Scheme.	63
13	Problem 4 Solutions for the LCMOT Scheme.	64
14	Problem 4 Error vs. Epsilon for the LCMOT Scheme.	65

LIST OF TABLES

<u>Table</u>		<u>Page</u>
1	Test Problem 1	54
2	Test Problem 2	56
3	SI vs. DSA for LCMOT	57
4	Test Problem 3	57
5	Test Problem 3'	58
6	SI vs. DSA for LCMOT	60
7	SI vs. DSA for LCMOT	65

ANALYSIS OF THE METHOD OF TUBES CHARACTERISTIC SCHEMES IN THE THICK DIFFUSIVE LIMIT

1 INTRODUCTION

For many years there has been wide interest in the neutral particle transport community involving optically thick and diffusive problems. In general, neutron transport problems are relatively thin and intermediate in optical thickness. Unlike neutron transport problems, electron and thermal radiative transfer problems are more likely to be optically thick and diffusive where particles undergo many collisions with few of those collisions removing the particle from the system. There are many examples to solving electron and thermal radiative transfer problems with applications in: astrophysics, inertial confinement fusion, atmospheric science, glass manufacturing, etc.

There are many very detailed techniques for solving some of these problems. These techniques can be divided into three general categories: deterministic, Implicit Monte Carlo and hybrid. Each category has its own advantages and disadvantages. Deterministic methods involve discretizing the particle transport equation in each of the phase-space variables. Deterministic methods are often computationally inexpensive and naturally provide solutions everywhere in the problem domain. These methods can have discretization error due to the approximations made and the coarseness of the spatial discretization. Monte Carlo methods involve simulating the individual histories of radiation particles. There has been recent work done in developing hybrid methods which have characteristics of both the deterministic and Monte Carlo methods.

Within the deterministic methods category there are many different ways to

discretize the analytic transport equation. These methods include finite volume, finite difference and finite element methods which have been very extensively researched in the heat transfer and fluid transport community. Instead of using one of these methods, we would like to choose a method that gives us the highest accuracy possible for a given number of unknowns. For this, we choose to investigate the characteristic methods approach. This is done by analytically inverting the streaming-plus-collision operator and making an approximation of the scattering source shape. By making as few approximations as possible, we have conserved as much accuracy as possible while introducing the fewest spatial unknowns.

Applying the deterministic method to an optically thick and diffusive problem can lead to some challenges. Particularly, the solutions converge slowly when using the standard source iteration method. There are, however, several ways of either preconditioning or accelerating the source iteration so that the solution will converge more quickly.

The remainder of this chapter consists of a literature review and an overview of the remainder of this thesis. The literature review provides an overview of publications on spherical geometry particle transport in thick diffusive regions and diffusion synthetic acceleration methods.

1.1 Literature Review

In this section of the thesis we review literature involving spherical geometry transport, characteristic methods, optically thick and diffusive problems and diffusion synthetic acceleration techniques. There has been work involving spherical geometry transport, especially in how the radial and angular streaming terms have been dealt with. Also, some of this work has been directly related to optically

thick and diffusive regimes. We will be presenting a new family of characteristic methods that can be applied to spherical geometry transport for optically thick problems.

1.1.1 Characteristic Transport Methods in Thick, Diffusive Regimes

Transport discretizations that involve the inversion of the “streaming plus collision” operator along the direction of particle travel, given an assumed spatial shape of the total source (scattering source plus external source) are known as *characteristic methods* in the radiation transport literature. In general, there are two classes of these methods: short characteristics, where interpolation is performed to calculate the angular fluxes on the incident surfaces of each spatial cell, and long characteristics, where the solution is computed through the entire domain without interpolation from incident problem boundary surfaces to exiting problem boundary surfaces. Long characteristics methods in Cartesian geometries are often used to compute the neutron flux, power distributions and assembly-averaged cross sections in nuclear reactor fuel assemblies [Smi 02]. One advantage of characteristic methods is that, in comparison with other types of transport spatial discretizations (finite volume, finite difference and finite element), they often have the smallest spatial truncation error for a fixed number of spatial unknowns per cell.

Reactor physics problems do not typically involve spatial zoning or material properties that would cause them to be classified as optically thick and diffusive, unlike many radiative transfer problems of interest. Adams et al [Ada 98] studied the behavior of a family of short characteristics methods in Cartesian geometries in optically thick, diffusive regions, and found that for certain spatial representations of the total source and cell-surface interpolations, very accurate results are possible.

It has long been known that transport theory transitions to diffusion theory under certain conditions. The process used to mathematically confirm this conjecture is known as an “asymptotic analysis” and has been illustrated in many places in the literature [Lar 86, Lar 90]. This technique involves a scaling of the transport equation by a small parameter ε . This scaling mathematically details the special group of problems with which we are concerned; namely optically thick ($\frac{\sigma_a t}{\varepsilon} \gg 1$) and diffusive ($\varepsilon \sigma_a \ll 1$) problems.

1.1.2 1-D Spherical Geometry Characteristic Methods

While the bulk of the development of characteristic methods has been performed in Cartesian geometries, there are several papers that describe characteristic methods in curvilinear geometries. The earliest references to these methods involve discretizations in spherical geometry [Vla 58], [Ask 72], [Nik 72]. Askew [Ask 72] is likely the first to have referred to the use of “tubes” in general-geometry step characteristic methods. In his work, a “tube” is the volume traced out as a surface area is translated along the path of particle travel. The vast majority of the work on these methods is in the Russian literature; Troschiev’s research group were the first to suggest a specific choice of tube geometry: These methods typically involve a transformation of the spherical geometry transport equation from the familiar r - μ space-angle coordinate system into either a one- or two-dimensional Cartesian coordinate system.

These characteristic methods have not been widely used in radiative heat transfer problems. The most common approach to the solution of the spherical geometry transport equation involves independent discretizations of the angular and radial variables. The angular variable is often treated with weighted diamond differenc-

ing (WDD) [Mor 84], allowing the spatial variable to be treated with WDD, the finite element method, or any other method of interest. Certain finite element schemes, in conjunction with WDD in angle, have been shown to yield accurate solutions in thick, diffusive regions [Pal 91]. Recently, Warsa and Morel [War 07] have developed a P_{N-1} - equivalent S_N angular discretization that avoids the need for the solution of a “starting direction” transport equation, and yields accurate results in thick diffusive regions.

1.1.3 Source Iteration and Diffusion Synthetic Acceleration

A vast majority of the work in deterministic transport has been done using a discrete ordinates (S_N) approach to accurately integrate the angular flux term in the source over a discrete number of angular directions. Even though the “Method of Tubes” isn’t strictly an S_N approach, the properties of the system of linear equations is very much the same. The most basic iterative approach to the solution of the linear system is Source Iteration (SI). This technique makes use of an estimate of the scalar flux (either an initial guess or previous iteration information) to compute the scattering source on the right-hand-side of the transport equation. A fixed source problem can be swept to obtain a new scalar flux estimate. This process is repeated until convergence on the scattering source is obtained. For systems with a low probability of leakage and high scattering ratio (optically thick and diffusive), the SI scheme converges very slowly leading to computational inefficiency. Also, there is a high likelihood of false convergence. This phenomenon occurs when the solution appears to have converged to the designated criteria only because the change in solution is extremely small [Ada 02]. In optically thick and diffusive problems, we have to protect against false convergence by tightening the

convergence criteria by several orders of magnitude.

In most radiative transfer simulations the standard SI scheme is preconditioned or accelerated. The definition of a preconditioning or acceleration scheme is that the solution is identical to the solution found from SI but is obtained in many fewer iterations. We are also protected against false convergence because the largest eigenvalue of the iteration operator is farther away from unity. In this research we have chosen to implement a version of Diffusion Synthetic Acceleration (DSA). This particular scheme determines the system of equations that govern the error of the SI solution and makes use of the P_1 diffusion approximation to simplify the DSA matrix [Ada 02]. Adams et al [Ada 98] showed that if a Finite Element Method (FEM) has the same asymptotic diffusion limit as a particular Characteristic Method (CM), the DSA scheme developed for the FEM can be applied to the CM.

1.2 Thesis Overview

The remainder of this thesis is organized as follows:

- II. In Chapter 2, we discuss the spherical geometry transport equation and the previous work that led to the transformation of the spherical geometry streaming operator to a slab-geometry-like streaming operator along the direction of particle travel.
- III. In Chapter 3, we introduce the “Method of Tubes” family of characteristic methods including the analytic inversion of the transformed streaming operator. Derivations of Nikofova’s original characteristic methods and the moment-based characteristic methods are included.

- IV. In Chapter 4, we perform an asymptotic diffusion analysis for all of the characteristic methods derived in the previous chapter. This analysis predicts how the methods will perform in optically thick and diffusive regions.
- V. In Chapter 5, we derive a DSA scheme that yields rapidly convergent solutions using the moment-based linear characteristic method. This acceleration scheme is derived using a linear discontinuous finite element transport method with the same asymptotic diffusion limit.
- VI. In Chapter 6, we present numerical results from the four derived characteristic methods. We solve several test problems and compare the solutions to the predictions of the asymptotic analysis.
- VII. In Chapter 7, we discuss the results in the previous chapter and conclude with suggestions for future work.

2 THE SPHERICAL GEOMETRY NEUTRAL PARTICLE TRANSPORT EQUATION

2.1 Introduction

The transport equation in 1-D spherical geometry in (r, μ) coordinates has the following conservative form:

$$\begin{aligned} \frac{\mu}{r^2} \frac{\partial}{\partial r} [r^2 \psi(r, \mu)] + \frac{1}{r} \frac{\partial}{\partial \mu} [(1 - \mu^2) \psi(r, \mu)] + \sigma_t(r) \psi(r, \mu) = \\ \frac{1}{2} \sigma_s(r) \int_{-1}^1 \psi(r, \mu') d\mu' + \frac{1}{2} q(r), \end{aligned}$$

$$0 \leq r \leq R, \quad -1 \leq \mu \leq 1, \quad (1)$$

with a specified incident angular flux outer boundary condition:

$$\psi(R, \mu) = \psi^{in}(\mu), \quad \mu < 0. \quad (2)$$

With the one-dimensional spherical geometry coordinate system shown in Figure (1), the quantities of interest only vary with the radial variable, \vec{r} . In this case, the angular variable, μ , shown in Eqs. (1) and (2) is defined,

$$\mu = \frac{\vec{\Omega} \cdot \vec{r}}{|\vec{r}|}. \quad (3)$$

Using the following relationship,

$$\frac{d\psi}{d\ell} = \frac{dr}{d\ell} \frac{\partial \psi}{\partial r} + \frac{d\mu}{d\ell} \frac{\partial \psi}{\partial \mu}, \quad (4)$$

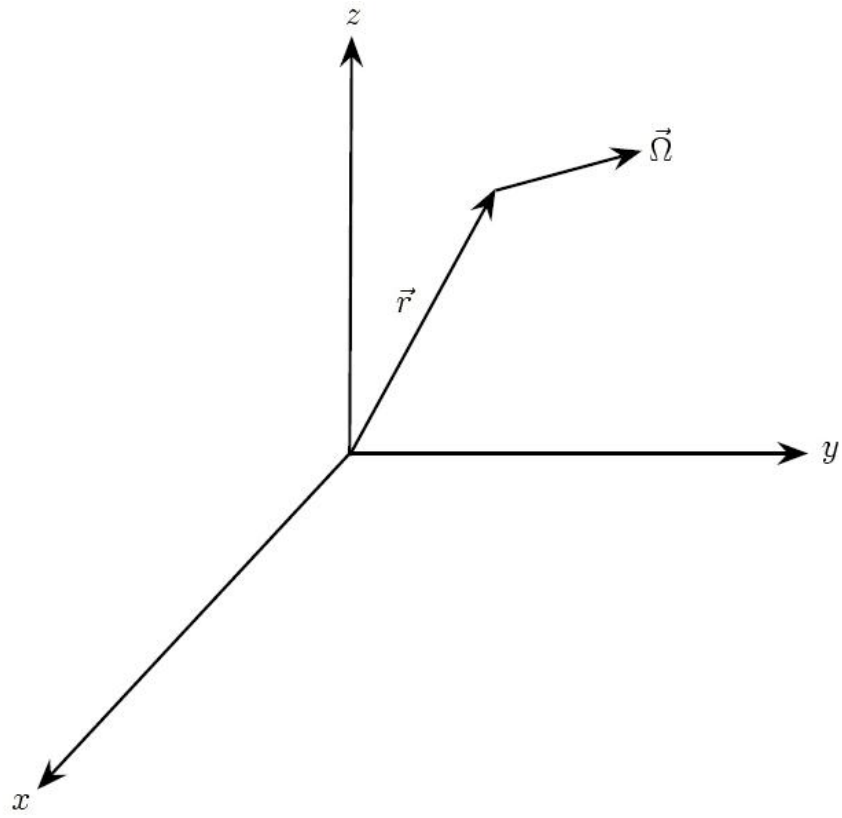


Figure 1: 1-D Spherical Geometry Coordinate System.

we can transform the streaming operator from Eq. (1) into a total derivative with respect to a coordinate along the direction of particle travel. ℓ is defined as the distance a particle travels along its characteristic pathway. Characteristic curves defined by

$$c = r\sqrt{1 - \mu^2}, \quad (5)$$

where c is a constant, are a consequence of the following relationships:

$$\frac{dr}{d\ell} = \mu, \quad (6)$$

$$\frac{d\mu}{d\ell} = \frac{(1 - \mu^2)}{r}. \quad (7)$$

The spherical geometry transport equation (Eq. (1)) in the ℓ coordinate is a slab-geometry-like equation:

$$\frac{d}{d\ell}\psi(\ell) + \sigma\psi(\ell) = \frac{1}{2}\sigma_s\phi(\ell) + \frac{1}{2}q(\ell). \quad (8)$$

2.2 Space-Angle Discretization

Given the transport equation in the transformed coordinate and the constant which defines the characteristic curves (Eq. (5)) we can introduce the space-angle grid shown in Fig. (2). Notice that the number of cells in the angular coordinate is completely determined given a choice of spatial mesh.

Before deriving the characteristic methods, we present important concepts from previous work [Nik 72]. Fig. (3) illustrates the phase-space cell (t, i) that is the

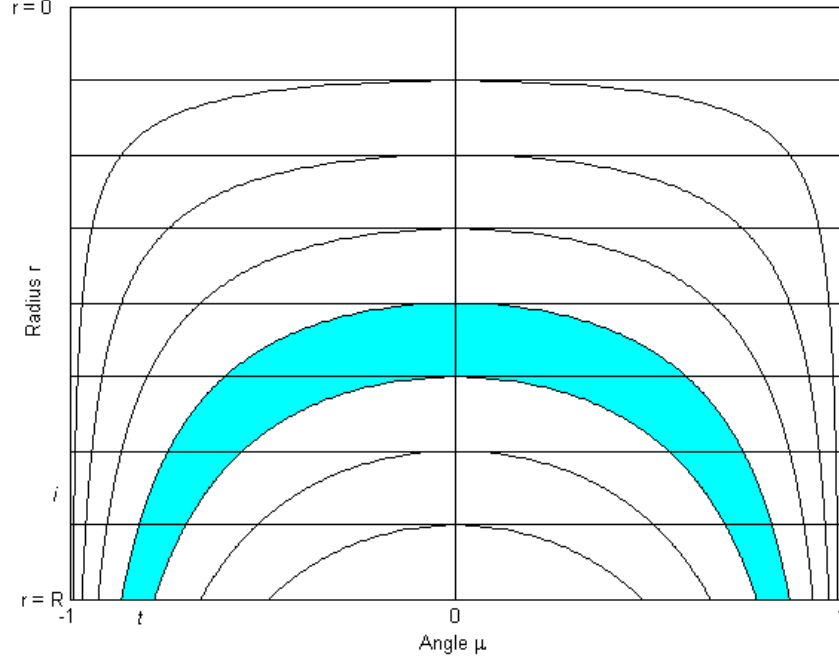


Figure 2: Discretized Space-Angle Grid in (r, μ) Coordinates.

fundamental discretization volume. The average characteristic path length within the volume element (t, i) is defined as $\Delta \ell_{t,i}$ and is shown in Eq. (9).

$$\Delta \ell_{t,i} = -\frac{\Delta_{t,i}}{r_{i+1/2}^2 \mu_{t,i+1/2} \Delta \mu_{t,i+1/2}} = -\frac{\Delta_{t,i}}{r_{i-1/2}^2 \mu_{t,i-1/2} \Delta \mu_{t,i-1/2}} \quad (9)$$

The $\Delta_{t,i}$ term is defined as the volume of element (t, i) and is defined,

$$\begin{aligned} \Delta_{t,i} = & \frac{1}{3} r_{i+1/2}^3 (\mu_{t+1/2,i+1/2}^3 - \mu_{t-1/2,i+1/2}^3) \\ & - \frac{1}{3} r_{i-1/2}^3 (\mu_{t+1/2,i-1/2}^3 - \mu_{t-1/2,i-1/2}^3) . \end{aligned} \quad (10)$$

Substituting Eq. (10) into Eq. (9), and performing some algebraic manipulation leads to the following equation for the average characteristic path length $\Delta \ell_{t,i}$,

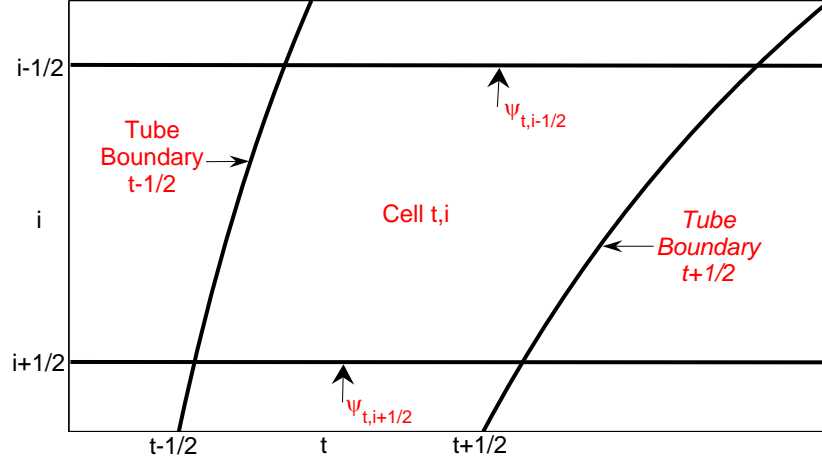


Figure 3: Phase Space Volume Element (t, i) in (r, μ) Coordinates.

$$\begin{aligned} \Delta \ell_{t,i} = & -\frac{2}{3} r_{i+1/2} \frac{\mu_{t+1/2,i+1/2}^2 + \mu_{t+1/2,i+1/2} \mu_{t-1/2,i+1/2} + \mu_{t-1/2,i+1/2}^2}{\mu_{t+1/2,i+1/2} + \mu_{t-1/2,i+1/2}} \\ & + \frac{2}{3} r_{i-1/2} \frac{\mu_{t+1/2,i-1/2}^2 + \mu_{t+1/2,i-1/2} \mu_{t-1/2,i-1/2} + \mu_{t-1/2,i-1/2}^2}{\mu_{t+1/2,i-1/2} + \mu_{t-1/2,i-1/2}}. \end{aligned} \quad (11)$$

The volumetric angular weight for cell (t, i) is used to calculate the spatial average and slope of the scalar flux in each cell. The relationships between the average and slope of the scalar flux and the average and slope of the angular flux are shown in Eqs. (12) and (13), respectively, and the edge net current is defined by Eq. (14).

$$\phi_i = \sum_t \psi_{t,i} \frac{\Delta_{t,i}}{\Delta V_i}, \quad (12)$$

$$\phi_i^x = \sum_t \psi_{t,i}^x \frac{\Delta_{t,i}}{\Delta V_i}, \quad (13)$$

$$J_{i\pm 1/2} = \sum_t \psi_{t,i\pm 1/2} \mu_{t,i\pm 1/2} \Delta \mu_{t,i\pm 1/2}. \quad (14)$$

Here the angle, $\mu_{t,i\pm 1/2}$, is defined by,

$$\mu_{t,i\pm 1/2} = \frac{1}{2} (\mu_{t+1/2,i\pm 1/2} + \mu_{t-1/2,i\pm 1/2}), \quad (15)$$

and the angular weight, $\Delta \mu_{t,i\pm 1/2}$, is defined by,

$$\Delta \mu_{t,i} = |\mu_{t+1/2,i\pm 1/2} - \mu_{t-1/2,i\pm 1/2}|. \quad (16)$$

ΔV_i is defined as the total volume across all tubes and is defined,

$$\Delta V_i = \int_{r_{i-1/2}}^{r_{i+1/2}} r^2 dr = \frac{1}{3} (r_{i+1/2}^3 - r_{i-1/2}^3). \quad (17)$$

In the next chapter we will describe a family of discretizations of the transport equation in ℓ -space (Eq. (8)). In particular, characteristic methods which involve analytically inverting the streaming-plus-collision operator yielding methods with relatively high orders of accuracy.

3 THE “METHOD OF TUBES” FAMILY OF CHARACTERISTIC METHODS

3.1 Introduction

This section contains a derivation of the Method of Tubes (MOT) family of characteristic methods. Starting with Eq. (8), we use an integrating factor of $\{e^{\sigma t \ell}\}$ to analytically invert the “streaming-plus-collision operator” in ℓ -space over a spatial cell,

$$\psi_{t,i+1/2} e^{\sigma_i \ell_{t,i+1/2}} - \psi_{t,i-1/2} e^{\sigma_i \ell_{t,i-1/2}} = \frac{1}{2} \int_{\ell_{t,i-1/2}}^{\ell_{t,i+1/2}} e^{\sigma_i \ell'} [\sigma_{s_i} \phi(\ell') + q(\ell')] d\ell'. \quad (18)$$

Members of the MOT family differ in the treatment of the spatial shape of the total source in the cell (scattering source and external source). We approximate the total source in Eq. (18) as a constant or a linear function across a spatial cell for the step and linear characteristic methods, respectively. The source approximation for the step characteristic method is,

$$Q(\ell) = \bar{Q}_i, \quad (19)$$

where,

$$Q(\ell) = \sigma_s \phi(\ell) + q(\ell). \quad (20)$$

By knowing the shape of the source, we can perform the integral on the right-hand-side of Eq. (18). The equations for a constant source will be referred to as the characteristic equations for the step characteristic methods (MOT-SS and

SCMOT). These equations can be used to compute angular fluxes and net currents on the outgoing face of the tube section. The outgoing angular fluxes are defined by,

$$\psi_{t,i+1/2} = \psi_{t,i-1/2} e^{-\sigma_i \Delta \ell_{t,i}} + \frac{\bar{Q}_i}{2\sigma_i} [1 - e^{-\sigma_i \Delta \ell_{t,i}}], \quad \Delta \ell_{t,i} > 0, \quad (21)$$

and,

$$\psi_{t,i-1/2} = \psi_{t,i+1/2} e^{\sigma_i \Delta \ell_{t,i}} + \frac{\bar{Q}_i}{2\sigma_i} [1 - e^{\sigma_i \Delta \ell_{t,i}}], \quad \Delta \ell_{t,i} < 0. \quad (22)$$

If the source is approximated as a linear function,

$$Q(\ell) = \bar{Q}_i + Q_i^x P_1(\ell), \quad (23)$$

where,

$$Q^x(\ell) = \sigma_s \phi^x(\ell) + q^x(\ell), \quad (24)$$

and,

$$P_1(\ell) = \frac{2(\ell - \ell_{t,i})}{\Delta \ell_{t,i}}, \quad (25)$$

the resulting equations are the characteristic equations for the linear characteristic methods (MOT-LS and LCMOT). The outgoing angular fluxes are computed from the equations,

$$\begin{aligned} \psi_{t,i+1/2} = & \psi_{t,i-1/2} e^{-\sigma_i \Delta \ell_{t,i}} + \frac{\bar{Q}_i}{2\sigma_i} [1 - e^{-\sigma_i \Delta \ell_{t,i}}] \\ & + \frac{Q_i^x}{2\sigma_i} \left[\left(1 - \frac{2}{\sigma_i \Delta \ell_{t,i}}\right) + \left(1 + \frac{2}{\sigma_i \Delta \ell_{t,i}}\right) e^{-\sigma_i \Delta \ell_{t,i}} \right], \quad \Delta \ell_{t,i} > 0, \end{aligned} \quad (26)$$

and,

$$\begin{aligned} \psi_{t,i-1/2} = & \psi_{t,i+1/2} e^{\sigma_i \Delta \ell_{t,i}} + \frac{\bar{Q}_i}{2\sigma_i} [1 - e^{\sigma_i \Delta \ell_{t,i}}] \\ & - \frac{Q_i^x}{2\sigma_i} \left[\left(1 + \frac{2}{\sigma_i \Delta \ell_{t,i}}\right) + \left(1 - \frac{2}{\sigma_i \Delta \ell_{t,i}}\right) e^{\sigma_i \Delta \ell_{t,i}} \right], \quad \Delta \ell_{t,i} < 0. \end{aligned} \quad (27)$$

Lastly, we can solve the transport equation along the characteristic pathway ($\mu = -1, r = 0, \mu = 1$). Because we know the angular values, $\mu = \pm 1$, we can remove the angular derivative term in the spherical transport equation (Eq. (1)) and write,

$$\mu \frac{\partial \psi(r, \mu)}{\partial r} + \sigma(r) \psi(r, \mu) = \frac{\sigma_s(r)}{2} \phi(r) + \frac{1}{2} q(r). \quad (28)$$

Using the integrating factor, $e^{\sigma(r)r/\mu}$, and assuming the source shape to be constant we find the characteristic equations for both positive and negative directions,

$$\psi_{i+1/2} = \psi_{i-1/2} e^{-\sigma_i \Delta r_i} + \frac{\bar{Q}_i}{2\sigma_i} [1 - e^{-\sigma_i \Delta r_i}], \quad (29)$$

and,

$$\psi_{i-1/2} = \psi_{i+1/2} e^{-\sigma_i \Delta r_i} + \frac{\bar{Q}_i}{2\sigma_i} [1 - e^{-\sigma_i \Delta r_i}]. \quad (30)$$

If the source shape is linear we find the following characteristic equations for both positive and negative directions,

$$\begin{aligned} \psi_{i+1/2} = & \psi_{i-1/2} e^{-\sigma_i \Delta r_i} + \frac{\bar{Q}_i}{2\sigma_i} [1 - e^{-\sigma_i \Delta r_i}] \\ & + \frac{Q_i^x}{2\sigma_i} \left[\left(1 - \frac{2}{\sigma_i \Delta r_i}\right) + \left(1 + \frac{2}{\sigma_i \Delta r_i}\right) e^{-\sigma_i \Delta r_i} \right], \end{aligned} \quad (31)$$

and,

$$\begin{aligned} \psi_{i-1/2} = & \psi_{i+1/2} e^{-\sigma_i \Delta r_i} + \frac{\bar{Q}_i}{2\sigma_i} [1 - e^{-\sigma_i \Delta r_i}] \\ & - \frac{Q_i^x}{2\sigma_i} \left[\left(1 - \frac{2}{\sigma_i \Delta r_i}\right) + \left(1 + \frac{2}{\sigma_i \Delta r_i}\right) e^{-\sigma_i \Delta r_i} \right]. \end{aligned} \quad (32)$$

3.2 Original Method of Tubes Schemes

In the original paper by Nikofova et al [Nik 72], several source shape approximations are considered. The spatial cell-edge scalar fluxes are computed using Eq. (14) and the angular integrated balance equation is used to determine the cell-average scalar flux,

$$r_{i+1/2}^2 J_{i+1/2} - r_{i-1/2}^2 J_{i-1/2} + \sigma_i \phi_i \Delta V_i = Q_i \Delta V_i, \quad (33)$$

where the cell-average source (scattering and fixed), Q_i , is determined using information from the previous iteration.

The source approximation in the original work has either a linear or parabolic representation in ℓ -space,

$$\phi(\ell) = a + b\ell + c\ell^2. \quad (34)$$

In this research, we consider only constant or step ($b = 0$ and $c = 0$) and linear source shapes ($c = 0$).

In all variations of the source shape, the scalar flux distribution is normalized such that to determine the source terms for the following iteration.

$$\int_0^{\Delta\ell_{t,i}} \phi(\ell) \frac{\Delta_{t,i}}{\Delta\ell_{t,i}} d\ell = \phi_i \int_0^{\Delta\ell_{t,i}} \frac{\Delta_{t,i}}{\Delta\ell_{t,i}} d\ell \quad (35)$$

3.2.1 Original MOT Constant (Step) Source Method (MOT-SS)

In this version of the MOT, the source is a constant:

$$\phi(\ell) = a \quad (36)$$

The constant, a , is determined by forcing the average of the flux distribution to be equal to the scalar flux cell-averaged balance equation from Eq. (33):

$$\frac{1}{\Delta V_i} \int_0^{\Delta\ell_{t,i}} \phi(\ell) \frac{\Delta_{t,i}}{\Delta\ell_{t,i}} d\ell = \phi_i. \quad (37)$$

The closure equations (Eqs. (21) and (22)) and the balance equations (Eqs. (33) and (37)) completely define the MOT-SS scheme. This scheme is identical (as will be shown in a later section) to the moment-based step characteristic method (SCMOT) we have derived using the traditional slab geometry characteristics approach.

3.2.2 Original MOT Linear Source Method (MOT-LS)

In this version of the MOT, the source is a linear function of the ℓ -coordinate. The cell-edge scalar fluxes are used to define this interpolant:

$$\phi(\ell) = \left[\tilde{\phi}_i + \tilde{\phi}_i^x \frac{2(\ell - \ell_{t,i})}{\Delta \ell_{t,i}} \right] \gamma_i, \quad (38)$$

where,

$$\tilde{\phi}_i = \frac{\phi_{i+1/2} + \phi_{i-1/2}}{2}, \quad (39)$$

and,

$$\tilde{\phi}_i^x = \frac{\phi_{i+1/2} - \phi_{i-1/2}}{2}. \quad (40)$$

We enforce the condition of particle balance by requiring the average of the function to equal the flux from the angular integrated balance equation, ϕ_i . This implies,

$$\gamma_i = \frac{\phi_i}{\frac{1}{2}(\phi_{i+1/2} + \phi_{i-1/2})}, \quad (41)$$

and changes the interpolant to the following form,

$$\phi(\ell) = \phi_i + \phi_i^x \frac{2(\ell - \ell_{t,i})}{\Delta \ell_{t,i}}, \quad (42)$$

where,

$$\phi_i^x = \gamma_i \tilde{\phi}_i^x = \phi_i \frac{(\phi_{i+1/2} - \phi_{i-1/2})}{(\phi_{i+1/2} + \phi_{i-1/2})}. \quad (43)$$

The closure equations (Eqs. (26) and (27)) and the balance equations (Eqs. (33), (42) and (43)) completely define the MOT-LS scheme. This requires that we determine the scalar flux at the center of the sphere, $r = 0$, to compute the average and slope scalar fluxes for the next iteration. This is accomplished using the starting direction equations for the linear method (Eqs. (31) and (32)).

3.3 Moment-Based Method of Tubes Schemes

The standard methods for deriving characteristic methods in slab geometry involve taking spatial moments of the transport equation to determine the cell average angular flux quantities. From the cell average angular flux quantities, the cell average scalar flux quantities are calculated and substituted into the scattering source for the following iteration.

The moment-based methods use the same closure equations as the original MOT schemes. The constant (step) source method, SCMOT, makes use of the source approximation in Eq. (19), and the resulting closure equations (Eqs. (21) and (22)). The linear source method, LCMOT, makes use of the source approximation in Eq. (23), and the resulting closure equations (Eqs. (26) and (27)).

3.3.1 *Moment-Based Step Characteristic MOT (SCMOT)*

By taking the zero-th spatial moment of Eq. (8), we can determine the average angular flux in the cell. This value will be used to calculate the radial scalar flux shown in Eq. (12). This method of calculating the cell average scalar flux enforces conservation of the angular flux.

$$\int_{\ell_{t,i-1/2}}^{\ell_{t,i+1/2}} \frac{\partial}{\partial \ell'} \psi(\ell') d\ell' + \int_{\ell_{t,i-1/2}}^{\ell_{t,i+1/2}} \sigma_i \psi(\ell') d\ell' = \frac{1}{2} \int_{\ell_{t,i-1/2}}^{\ell_{t,i+1/2}} [\sigma_{si} \phi(\ell') + q(\ell')] d\ell' \quad (44)$$

Evaluating Eq. (44) leads to the balance equation,

$$\frac{[\psi_{t,i+1/2} - \psi_{t,i-1/2}]}{\Delta \ell_{t,i}} + \sigma_i \psi_{t,i} = \frac{1}{2} [\sigma_{si} \phi_i + q_i]. \quad (45)$$

Eqs. (12), (21), (22), and (45) define the angular flux conservative version of the step characteristic method of tubes (SCMOT). This method is actually identical to MOT-SS. If we operate on Eq. (45) by multiplying by the volumetric weights and summing over all tubes ($\sum_t \cdot \frac{\Delta_{t,i}}{\Delta V_i}$) we end up with the zero-th angular moment of the balance equation (Eq. (33)).

3.3.2 Moment-Based Linear Characteristic MOT (LCMOT)

This method requires equations for the average angular flux, $\psi_{t,i}$, and the slope of the angular flux, $\psi_{t,i}^x$. By taking both the zero-th (Eq.(45)) and the first spatial moment of Eq. (8) we can generate equations to compute these two quantities. These angular flux moments will be used to calculate the average scalar flux, ϕ_i , shown in Eq. (12) and the scalar flux slope, ϕ_i^x , shown in Eq. (13). The first spatial moment equation involves multiplying Eq. (8) by the P_1 function in Eq. (25) and integrating over a tube subcell.

$$\begin{aligned} & \int_{\ell_{t,i-1/2}}^{\ell_{t,i+1/2}} P_1(\ell) \frac{\partial}{\partial \ell'} \psi(\ell') d\ell' + \int_{\ell_{t,i-1/2}}^{\ell_{t,i+1/2}} P_1(\ell) \sigma_i \psi(\ell') d\ell' \\ &= \frac{1}{2} \int_{\ell_{t,i-1/2}}^{\ell_{t,i+1/2}} P_1(\ell) [\sigma_{si} \phi(\ell') + q(\ell')] d\ell' \end{aligned} \quad (46)$$

Evaluating Eq. (46) leads to a balance equation for the slope,

$$\frac{3[\psi_{t,i+1/2} + \psi_{t,i-1/2} - 2\psi_{t,i}]}{\Delta\ell_{t,i}} + \sigma_i\psi_{t,i}^x = \frac{1}{2}[\sigma_{s_i}\phi_i^x + q_i^x]. \quad (47)$$

Eqs. (12), (13), (26), (27), (45) and (47) define the angular flux conservation version of the linear characteristic method of tubes (LCMOT).

4 ASYMPTOTIC DIFFUSION ANALYSIS

4.1 Introduction

We review this material by considering the behavior of the exact spherical geometry transport equation in optically thick and diffusive regions. If the cross-sections and sources are appropriately scaled such that the medium is optically thick and scattering-dominated,

$$\sigma_t \rightarrow \frac{1}{\varepsilon} \sigma_t, \quad \sigma_a \rightarrow \varepsilon \sigma_a, \quad q \rightarrow \varepsilon q, \quad (48)$$

the solution of the transport equation in the interior of this medium (to leading order) satisfies a diffusion equation. It is necessary for the angular and scalar flux solutions, and the net current solution to be expanded in power series of ε ,

$$\psi = \sum_{m=0}^{\infty} \varepsilon^m \psi^{[m]}, \quad \phi = \sum_{m=0}^{\infty} \varepsilon^m \phi^{[m]}, \quad J = \sum_{m=0}^{\infty} \varepsilon^m J^{[m]}, \quad (49)$$

We begin with scaled versions of Eqs. (1) and (2),

$$\frac{\mu}{r^2} \frac{\partial}{\partial r} [r^2 \psi(r, \mu)] + \frac{1}{r} \frac{\partial}{\partial \mu} [(1 - \mu^2) \psi(r, \mu)] + \frac{\sigma_t(r)}{\varepsilon} \psi(r, \mu) =$$

$$\frac{1}{2} \left(\frac{\sigma_t(r)}{\varepsilon} - \varepsilon \sigma_a(r) \right) \int_{-1}^1 \psi(r, \mu') d\mu' + \frac{\varepsilon}{2} q(r),$$

$$0 \leq r \leq R, \quad -1 \leq \mu \leq 1, \quad (50)$$

$$\psi(R, \mu) = \psi^{in}(\mu), \quad \mu < 0. \quad (51)$$

We ask how the solution behaves as ε tends toward zero. We find that in the interior of the diffusive region, the leading-order angular flux is *isotropic* and satisfies a *diffusion equation*:

$$\psi(r, \mu) = \frac{1}{2} \phi(r) + O(\varepsilon), \quad (52)$$

$$-\frac{1}{r^2} \frac{d}{dr} \left(\frac{r^2}{3\sigma_t(r)} \frac{d\phi(r)}{dr} \right) + \sigma_a(r)\phi(r) = q(r), \quad (53)$$

with “transport-corrected” boundary conditions,

$$\phi(R) = 2 \int_{-1}^0 d\mu W(|\mu|) \psi^{in}(\mu). \quad (54)$$

This boundary condition (Eq. (54)) is a Dirichlet condition equal to a weighted integral of the incoming angular flux on the outer surface of the sphere, $\psi^{in}(\mu)$. The weight function, $W(\mu)$, is defined in terms of Chandrasekhar’s H function for a purely scattering medium[Cha 60]:

$$\begin{aligned} W(\mu) &= \frac{\sqrt{3}}{2} \mu H(\mu) \\ &= 0.91\mu + 1.635\mu^2 \pm \text{a few \%} \\ &\approx \mu + \frac{3}{2}\mu^2. \end{aligned} \quad (55)$$

These results serve to motivate the use of this asymptotic analysis as a tool in determining whether *discretized* spherical geometry transport equations transition to accurate *discretized* diffusion equations (with accurate boundary conditions) in thick regions. If so, and if the spatial grid is fine enough to resolve the diffusion

solution, we claim that the transport discretization is accurate in thick, diffusive regions.

4.2 Asymptotic Analysis Procedure

We perform an asymptotic analysis of both original methods (MOT-SS and MOT-LS) and both moment-based methods (SCMOT and LCMOT), defined in the previous chapter, to predict their behavior in optically thick and diffusive regions. If the discretized transport equations in these optically thick and diffusive regions 1) yield accurate discretizations of the diffusion equations, with 2) accurate boundary conditions then we say that the transport methods are well-behaved in the thick, diffusion limit.

The analyses in each of the next subsections follows the same procedure. We define a small parameter ε , introduce scaled cross sections and sources (Eq. (48)), introduce power series expansions of the solutions (Eq. (49)), and consider the transport problem as $\varepsilon \rightarrow 0$.

4.2.1 Analysis of MOT-SS

Applying the asymptotic analysis procedure to Eqs. (21), (22), and (33) of the MOT-SS discretized equations leads to the following scaled, discretized transport equations,

$$\sum_{m=0}^{\infty} \varepsilon^m \psi_{t,i+1/2}^{[m]} = \frac{(\sigma_i - \varepsilon^2 \sigma_{ai}) \sum_{m=0}^{\infty} \varepsilon^m \phi_i^{[m]} + \varepsilon^2 q_i}{2\sigma_i}, \quad \Delta \ell_{t,i} > 0, \quad (56)$$

$$\sum_{m=0}^{\infty} \varepsilon^m \psi_{t,i-1/2}^{[m]} = \frac{(\sigma_i - \varepsilon^2 \sigma_{ai}) \sum_{m=0}^{\infty} \varepsilon^m \phi_i^{[m]} + \varepsilon^2 q_i}{2\sigma_i}, \quad \Delta \ell_{t,i} < 0, \quad (57)$$

and,

$$\begin{aligned} & \left[r_{i+1/2}^2 \sum_{m=0}^{\infty} \varepsilon^m J_{i+1/2}^{[m]} - r_{i-1/2}^2 \sum_{m=0}^{\infty} \varepsilon^m J_{i-1/2}^{[m]} \right] + \frac{\sigma_i}{\varepsilon} \Delta V_i \sum_{m=0}^{\infty} \varepsilon^m \phi_i^{[m]} \\ & = \Delta V_i \left[\left(\frac{\sigma_i}{\varepsilon} - \varepsilon \sigma_{ai} \right) \sum_{m=0}^{\infty} \varepsilon^m \phi_i^{[m]} + \varepsilon q_i \right]. \end{aligned} \quad (58)$$

Note that the term, $e^{-|\sigma_i \Delta \ell_{t,i}|/\varepsilon}$, tends toward zero much more rapidly than does, $1/\varepsilon$. When the exponential term appears, we conclude there is no impact on the leading order solution, therefore, it is omitted. By equating the scaled, discretized equations in terms of order of ε we find from Eqs. (56), (57) and (58), respectively, the $O(\varepsilon^0)$ equations,

$$\psi_{t,i+1/2}^{[0]} = \frac{1}{2} \phi_i^{[0]}, \quad \Delta \ell_{t,i} > 0, \quad (59)$$

$$\psi_{t,i-1/2}^{[0]} = \frac{1}{2} \phi_i^{[0]}, \quad \Delta \ell_{t,i} < 0, \quad (60)$$

and,

$$\left[r_{i+1/2}^2 J_{i+1/2}^{[0]} - r_{i-1/2}^2 J_{i-1/2}^{[0]} \right] = 0. \quad (61)$$

Eqs. (59) and (60) are multiplied by the ratio of the volumetric weight to the average characteristic pathlength and summed over all tubes ($\sum_t \cdot \frac{\Delta_{t,i}}{\Delta \ell_{t,i}}$) to yield,

$$\sum_t \psi_{t,i+1/2}^{[0]} \frac{\Delta_{t,i}}{\Delta \ell_{t,i}} = r_{i+1/2}^2 J_{i+1/2}^{[0]} = \sum_{\Delta \ell_{t,i} > 0} \frac{1}{2} \phi_i^{[0]} \frac{\Delta_{t,i}}{\Delta \ell_{t,i}} + \sum_{\Delta \ell_{t,i} < 0} \frac{1}{2} \phi_{i+1}^{[0]} \frac{\Delta_{t,i}}{\Delta \ell_{t,i}}, \quad (62)$$

and,

$$\sum_t \psi_{t,i-1/2}^{[0]} \frac{\Delta_{t,i}}{\Delta \ell_{t,i}} = r_{i-1/2}^2 J_{i-1/2}^{[0]} = \sum_{\Delta \ell_{t,i} > 0} \frac{1}{2} \phi_{i-1}^{[0]} \frac{\Delta_{t,i}}{\Delta \ell_{t,i}} + \sum_{\Delta \ell_{t,i} < 0} \frac{1}{2} \phi_i^{[0]} \frac{\Delta_{t,i}}{\Delta \ell_{t,i}}. \quad (63)$$

The symmetry of the space-angle mesh implies,

$$r_{i+1/2}^2 J_{i+1/2}^{[0]} = \frac{1}{2} r_{i+1/2}^2 (\phi_i^{[0]} - \phi_{i+1}^{[0]}) \sum_{\mu_{t,i+1/2} > 0} \mu_{t,i+1/2} \Delta \mu_{t,i+1/2}, \quad (64)$$

and,

$$r_{i-1/2}^2 J_{i-1/2}^{[0]} = \frac{1}{2} r_{i-1/2}^2 (\phi_{i-1}^{[0]} - \phi_i^{[0]}) \sum_{\mu_{t,i-1/2} > 0} \mu_{t,i-1/2} \Delta \mu_{t,i-1/2}. \quad (65)$$

Substituting Eqs. (64) and (65) into Eq. (61), we find that the leading-order cell-average scalar flux in the interior of the problem, $1 \leq i < I$, satisfies the following equation:

$$\begin{aligned} & - \left[r_{i-1/2}^2 \sum_{\mu_{t,i-1/2} > 0} \mu_{t,i-1/2} \Delta \mu_{t,i-1/2} \right] \phi_{i-1}^{[0]} - \left[r_{i+1/2}^2 \sum_{\mu_{t,i+1/2} > 0} \mu_{t,i+1/2} \Delta \mu_{t,i+1/2} \right] \phi_{i+1}^{[0]} \\ & + \left[r_{i-1/2}^2 \sum_{\mu_{t,i-1/2} > 0} \mu_{t,i-1/2} \Delta \mu_{t,i-1/2} + r_{i+1/2}^2 \sum_{\mu_{t,i+1/2} > 0} \mu_{t,i+1/2} \Delta \mu_{t,i+1/2} \right] \phi_i^{[0]} = 0. \end{aligned} \quad (66)$$

Note that Eq. (66) is *not* a diffusion equation. At this point, it is clear that the method will perform very poorly in optically thick and diffusive regions.

For completeness, we also derive equations satisfied by the fluxes in the boundary cells, $i = 1$ and $i = I$. The innermost radius for each tube at $\mu = 0$, the boundary condition is defined by the net current equaling zero (reflecting boundary). The exterior boundary condition is a specified incident angular flux condition.

$$\psi_{t,i+1/2}^{[0]} = g_t, \quad \Delta\ell_{t,i} < 0, \quad i = I \quad (67)$$

Eqs. (59) and (60) on the innermost boundary edge are multiplied by the ratio of the volumetric weight to the average characteristic pathlength and summed over all tubes to yield,

$$\sum_t \psi_{t,1/2}^{[0]} \frac{\Delta_{t,1}}{\Delta\ell_{t,1}} = 0 = \sum_{\Delta\ell_{t,1} > 0} \frac{1}{2} \phi_0^{[0]} \frac{\Delta_{t,1}}{\Delta\ell_{t,1}} + \sum_{\Delta\ell_{t,1} < 0} \frac{1}{2} \phi_1^{[0]} \frac{\Delta_{t,1}}{\Delta\ell_{t,1}}. \quad (68)$$

This leads to the following solution for the interior cell:

$$\phi_0^{[0]} - \phi_1^{[0]} = 0. \quad (69)$$

Lastly, for cell $i = I$, we use the incident angular flux boundary condition in Eq. (67) and operate on Eqs. (59) and (60) by multiplying by the ratio of the volumetric weight to the average characteristic pathlength and summing over all tubes:

$$\sum_t \psi_{t,I+1/2}^{[0]} \frac{\Delta_{t,I}}{\Delta\ell_{t,I}} = \sum_{\Delta\ell_{t,I} > 0} \frac{1}{2} \phi_I^{[0]} \frac{\Delta_{t,I}}{\Delta\ell_{t,I}} + \sum_{\Delta\ell_{t,I} < 0} g_t \frac{\Delta_{t,I}}{\Delta\ell_{t,I}}, \quad (70)$$

and,

$$\sum_t \psi_{t,I-1/2}^{[0]} \frac{\Delta_{t,I}}{\Delta\ell_{t,I}} = \sum_{\Delta\ell_{t,I} > 0} \frac{1}{2} \phi_{I-1}^{[0]} \frac{\Delta_{t,I}}{\Delta\ell_{t,I}} + \sum_{\Delta\ell_{t,I} < 0} \frac{1}{2} \phi_I^{[0]} \frac{\Delta_{t,I}}{\Delta\ell_{t,I}}. \quad (71)$$

This leads to the following solution for the outermost cell,

$$\begin{aligned}
& - \left[r_{I-1/2}^2 \sum_{\mu_{t,I-1/2} > 0} \mu_{t,I-1/2} \Delta \mu_{t,I-1/2} \right] \phi_{I-1}^{[0]} \\
& + \left[r_{I-1/2}^2 \sum_{\mu_{t,I-1/2} > 0} \mu_{t,I-1/2} \Delta \mu_{t,I-1/2} + r_{I+1/2}^2 \sum_{\mu_{t,I+1/2} > 0} \mu_{t,I+1/2} \Delta \mu_{t,I+1/2} \right] \phi_I^{[0]} \\
& = r_{I+1/2}^2 \sum_{\mu_{t,I+1/2} > 0} g_t \mu_{t,I+1/2} \Delta \mu_{t,I+1/2} .
\end{aligned} \tag{72}$$

Eqs. (66), (69), and (72) are a tridiagonal system of linear equations which predict the behavior of the MOT-SS transport method in optically thick and diffusive regions. The leading-order scalar fluxes from the MOT-SS are completely independent of cross sections, sources and mesh spacing. The boundary conditions completely dictate the solution on the interior of the problem which is unphysical. Observations of the behavior of this method confirm the results of this analysis - numerical solutions of MOT-SS tend toward zero as epsilon decreases for a problem with a vacuum outer boundary condition.

4.2.2 Analysis of SCMOT

Applying the asymptotic analysis procedure to Eqs. (21), (22), and (45) of the SCMOT discretized equations leads to the following scaled, discretized transport equations,

$$\sum_{m=0}^{\infty} \varepsilon^m \psi_{t,i+1/2}^{[m]} = \frac{(\sigma_i - \varepsilon^2 \sigma_{ai}) \sum_{m=0}^{\infty} \varepsilon^m \phi_i^{[m]} + \varepsilon^2 q_i}{2\sigma_i}, \quad \Delta l_{t,i} > 0, \tag{73}$$

$$\sum_{m=0}^{\infty} \varepsilon^m \psi_{t,i-1/2}^{[m]} = \frac{(\sigma_i - \varepsilon^2 \sigma_{ai}) \sum_{m=0}^{\infty} \varepsilon^m \phi_i^{[m]} + \varepsilon^2 q_i}{2\sigma_i}, \quad \Delta \ell_{t,i} < 0, \quad (74)$$

and,

$$\begin{aligned} & \frac{\left[\sum_{m=0}^{\infty} \varepsilon^m \psi_{t,i+1/2}^{[m]} - \sum_{m=0}^{\infty} \varepsilon^m \psi_{t,i-1/2}^{[m]} \right]}{\Delta \ell_{t,i}} + \frac{\sigma_i}{\varepsilon} \sum_{m=0}^{\infty} \varepsilon^m \psi_{t,i}^{[m]} \\ &= \frac{\frac{\sigma_i}{\varepsilon} - \varepsilon \sigma_{ai}}{2} \sum_{m=0}^{\infty} \varepsilon^m \phi_i^{[m]} + \frac{\varepsilon}{2} q_i. \end{aligned} \quad (75)$$

By equating the scaled, discretized equations in terms of order of ε we obtain the $O(\varepsilon^{-1})$ equation,

$$\psi_{t,i}^{[0]} = \frac{1}{2} \phi_i^{[0]}. \quad (76)$$

From Eqs. (73), (74) and (75), respectively, the $O(\varepsilon^0)$ equations are,

$$\psi_{t,i+1/2}^{[0]} = \frac{1}{2} \phi_i^{[0]}, \quad \Delta \ell_{t,i} > 0, \quad (77)$$

$$\psi_{t,i-1/2}^{[0]} = \frac{1}{2} \phi_i^{[0]}, \quad \Delta \ell_{t,i} < 0, \quad (78)$$

and,

$$\frac{\psi_{t,i+1/2}^{[0]} - \psi_{t,i-1/2}^{[0]}}{\Delta \ell_{t,i}} + \sigma_i \psi_{t,i}^{[1]} = \frac{\sigma_i}{2} \phi_i^{[1]}. \quad (79)$$

We operate on Eq. (79) by multiplying by the volumetric weight and summing over all tubes ($\sum_t \cdot \Delta \ell_{t,i}$) to find,

$$\sum_t \frac{(\psi_{t,i+1/2}^{[0]} - \psi_{t,i-1/2}^{[0]})}{\Delta \ell_{t,i}} \Delta_{t,i} = 0. \quad (80)$$

Operating on Eqs. (77) and (78) by multiplying by the ratio of the volumetric weight to the average characteristic pathlength and summing over all tubes yields,

$$\sum_t \psi_{t,i+1/2}^{[0]} \frac{\Delta_{t,i}}{\Delta \ell_{t,i}} = \sum_{\Delta \ell_{t,i} > 0} \frac{1}{2} \phi_i^{[0]} \frac{\Delta_{t,i}}{\Delta \ell_{t,i}} + \sum_{\Delta \ell_{t,i} < 0} \frac{1}{2} \phi_{i+1}^{[0]} \frac{\Delta_{t,i}}{\Delta \ell_{t,i}}, \quad (81)$$

and,

$$\sum_t \psi_{t,i-1/2}^{[0]} \frac{\Delta_{t,i}}{\Delta \ell_{t,i}} = \sum_{\Delta \ell_{t,i} > 0} \frac{1}{2} \phi_{i-1}^{[0]} \frac{\Delta_{t,i}}{\Delta \ell_{t,i}} + \sum_{\Delta \ell_{t,i} < 0} \frac{1}{2} \phi_i^{[0]} \frac{\Delta_{t,i}}{\Delta \ell_{t,i}}. \quad (82)$$

The symmetry of the space-angle mesh implies,

$$\sum_t \psi_{t,i+1/2}^{[0]} \frac{\Delta_{t,i}}{\Delta \ell_{t,i}} = \frac{1}{2} r_{i+1/2}^2 (\phi_i^{[0]} - \phi_{i+1}^{[0]}) \sum_{\mu_{t,i+1/2} > 0} \mu_{t,i+1/2} \Delta \mu_{t,i+1/2}, \quad (83)$$

and,

$$\sum_t \psi_{t,i-1/2}^{[0]} \frac{\Delta_{t,i}}{\Delta \ell_{t,i}} = \frac{1}{2} r_{i-1/2}^2 (\phi_{i-1}^{[0]} - \phi_i^{[0]}) \sum_{\mu_{t,i-1/2} > 0} \mu_{t,i-1/2} \Delta \mu_{t,i-1/2}. \quad (84)$$

Substituting Eqs. (83) and (84) into Eq. (80) we find that the leading-order cell-averaged scalar flux in the interior of the problem, $1 \leq i < I$, satisfies the following equation:

$$\begin{aligned}
& - \left[r_{i-1/2}^2 \sum_{\mu_{t,i-1/2} > 0} \mu_{t,i-1/2} \Delta \mu_{t,i-1/2} \right] \phi_{i-1}^{[0]} - \left[r_{i+1/2}^2 \sum_{\mu_{t,i+1/2} > 0} \mu_{t,i+1/2} \Delta \mu_{t,i+1/2} \right] \phi_{i+1}^{[0]} \\
& + \left[r_{i-1/2}^2 \sum_{\mu_{t,i-1/2} > 0} \mu_{t,i-1/2} \Delta \mu_{t,i-1/2} + r_{i+1/2}^2 \sum_{\mu_{t,i+1/2} > 0} \mu_{t,i+1/2} \Delta \mu_{t,i+1/2} \right] \phi_i^{[0]} = 0.
\end{aligned} \tag{85}$$

This interior result is the same as the result of the analysis for the MOT-SS.

For completeness, we also derive equations satisfied by the fluxes in the boundary cells, $i = 1$ and $i = I$. The innermost radius for each tube at $\mu = 0$, the boundary condition is that the current is zero (reflecting boundary). The exterior boundary condition is a specified incident isotropic angular flux condition.

$$\psi_{t,i+1/2}^{[0]} = g_t, \quad \Delta \ell_{t,i} < 0, \quad i = I \tag{86}$$

Eqs. (77) and (78) on the innermost boundary edge are multiplied by the ratio of the volumetric weight to the average characteristic pathlength and summed over all tubes to yield,

$$\sum_t \psi_{t,1/2}^{[0]} \frac{\Delta_{t,1}}{\Delta \ell_{t,1}} = 0 = \sum_{\Delta \ell_{t,1} > 0} \frac{1}{2} \phi_0^{[0]} \frac{\Delta_{t,1}}{\Delta \ell_{t,1}} + \sum_{\Delta \ell_{t,1} < 0} \frac{1}{2} \phi_1^{[0]} \frac{\Delta_{t,1}}{\Delta \ell_{t,1}}. \tag{87}$$

This leads to the following solution for the interior cell:

$$\phi_0^{[0]} - \phi_1^{[0]} = 0. \tag{88}$$

Lastly, for cell $i = I$, we use the incident angular flux boundary condition in Eq. (86) and operate on Eqs. (77) and (78) by multiplying by the ratio of the

volumetric weight to the average characteristic pathlength and summing over all tubes:

$$\sum_t \psi'_{t,I+1/2} \frac{\Delta_{t,I}}{\Delta \ell_{t,I}} = \sum_{\Delta \ell_{t,I} > 0} \frac{1}{2} \phi_I^{[0]} \frac{\Delta_{t,I}}{\Delta \ell_{t,I}} + \sum_{\Delta \ell_{t,I} < 0} g_t \frac{\Delta_{t,I}}{\Delta \ell_{t,I}}, \quad (89)$$

and,

$$\sum_t \psi_{t,I-1/2} \frac{\Delta_{t,I}}{\Delta \ell_{t,I}} = \sum_{\Delta \ell_{t,I} > 0} \frac{1}{2} \phi_{I-1}^{[0]} \frac{\Delta_{t,I}}{\Delta \ell_{t,I}} + \sum_{\Delta \ell_{t,I} < 0} \frac{1}{2} \phi_I^{[0]} \frac{\Delta_{t,I}}{\Delta \ell_{t,I}}. \quad (90)$$

This leads to the following solution for the outermost cell,

$$\begin{aligned} & - \left[r_{I-1/2}^2 \sum_{\mu_{t,I-1/2} > 0} \mu_{t,I-1/2} \Delta \mu_{t,I-1/2} \right] \phi_{I-1}^{[0]} \\ & + \left[r_{I-1/2}^2 \sum_{\mu_{t,I-1/2} > 0} \mu_{t,I-1/2} \Delta \mu_{t,I-1/2} + r_{I+1/2}^2 \sum_{\mu_{t,I+1/2} > 0} \mu_{t,I+1/2} \Delta \mu_{t,I+1/2} \right] \phi_I^{[0]} \\ & = r_{I+1/2}^2 \sum_{\mu_{t,I+1/2} > 0} g_t \mu_{t,I+1/2} \Delta \mu_{t,I+1/2}. \end{aligned} \quad (91)$$

The diffusion limit for SCMOT is equivalent to the diffusion limit shown for MOT-SS. This is more evidence that the two methods are equivalent.

4.2.3 Analysis of LCMOT

Applying the asymptotic analysis procedure to Eqs. (26), (27), (45) and (47) of the LCMOT leads to the following scaled, discretized transport equations,

$$\begin{aligned}
\sum_{m=0}^{\infty} \varepsilon^m \psi_{t,i+1/2}^{[m]} &= \frac{(\sigma_i - \varepsilon^2 \sigma_{ai}) \sum_{m=0}^{\infty} \varepsilon^m \phi_i^{[m]} + \varepsilon^2 q_i}{2\sigma_i} \\
&+ \left[\frac{(\sigma_i - \varepsilon^2 \sigma_{ai}) \sum_{m=0}^{\infty} \varepsilon^m \phi_i^{x[m]} + \varepsilon^2 q_i^x}{2\sigma_i} \right] \left[1 - \frac{2\varepsilon}{\sigma_i \Delta \ell_{t,i}} \right], \quad \Delta \ell_{t,i} > 0,
\end{aligned} \tag{92}$$

$$\begin{aligned}
\sum_{m=0}^{\infty} \varepsilon^m \psi_{t,i-1/2}^{[m]} &= \frac{(\sigma_i - \varepsilon^2 \sigma_{ai}) \sum_{m=0}^{\infty} \varepsilon^m \phi_i^{[m]} + \varepsilon^2 q_i}{2\sigma_i} \\
&- \left[\frac{(\sigma_i - \varepsilon^2 \sigma_{ai}) \sum_{m=0}^{\infty} \varepsilon^m \phi_i^{x[m]} + \varepsilon^2 q_i^x}{2\sigma_i} \right] \left[1 + \frac{2\varepsilon}{\sigma_i \Delta \ell_{t,i}} \right], \quad \Delta \ell_{t,i} > 0,
\end{aligned} \tag{93}$$

$$\begin{aligned}
&\frac{\left[\sum_{m=0}^{\infty} \varepsilon^m \psi_{t,i+1/2}^{[m]} - \sum_{m=0}^{\infty} \varepsilon^m \psi_{t,i-1/2}^{[m]} \right]}{\Delta \ell_{t,i}} + \frac{\sigma_i}{\varepsilon} \sum_{m=0}^{\infty} \varepsilon^m \psi_{t,i}^{[m]} \\
&= \frac{\frac{\sigma_i}{\varepsilon} - \varepsilon \sigma_{ai}}{2} \sum_{m=0}^{\infty} \varepsilon^m \phi_i^{[m]} + \frac{\varepsilon}{2} q_i.
\end{aligned} \tag{94}$$

and,

$$\begin{aligned}
&3 \frac{\left[\sum_{m=0}^{\infty} \varepsilon^m \psi_{t,i+1/2}^{[m]} + \sum_{m=0}^{\infty} \varepsilon^m \psi_{t,i-1/2}^{[m]} - 2 \sum_{m=0}^{\infty} \varepsilon^m \psi_{t,i}^{[m]} \right]}{\Delta \ell_{t,i}} + \frac{\sigma_i}{\varepsilon} \sum_{m=0}^{\infty} \varepsilon^m \psi_{t,i}^{x[m]} \\
&= \frac{\frac{\sigma_i}{\varepsilon} - \varepsilon \sigma_{ai}}{2} \sum_{m=0}^{\infty} \varepsilon^m \phi_i^{x[m]} + \frac{\varepsilon}{2} q_i^x.
\end{aligned} \tag{95}$$

By equating the scaled, discretized equations in terms of order of ε we obtain the $O(\varepsilon^{-1})$ equations,

$$\psi_{t,i}^{[0]} = \frac{1}{2}\phi_i^{[0]}, \quad (96)$$

and,

$$\psi_{t,i}^{x[0]} = \frac{1}{2}\phi_i^{x[0]}. \quad (97)$$

From Eqs. (92), (93), (94) and (95), respectively, the $O(\varepsilon^0)$ equations are,

$$\psi_{t,i+1/2}^{[0]} = \frac{1}{2}(\phi_i^{[0]} + \phi_i^{x[0]}), \quad \Delta\ell_{t,i} > 0, \quad (98)$$

$$\psi_{t,i-1/2}^{[0]} = \frac{1}{2}(\phi_i^{[0]} - \phi_i^{x[0]}), \quad \Delta\ell_{t,i} < 0, \quad (99)$$

$$\frac{\psi_{t,i+1/2}^{[0]} - \psi_{t,i-1/2}^{[0]}}{\Delta\ell_{t,i}} + \sigma_i\psi_{t,i}^{[1]} = \frac{\sigma_i}{2}\phi_i^{[1]}, \quad (100)$$

and,

$$\frac{3[\psi_{t,i+1/2}^{[0]} + \psi_{t,i-1/2}^{[0]} - 2\psi_{t,i}^{[0]}]}{\Delta\ell_{t,i}} + \sigma_i\psi_{t,i}^{x[1]} = \frac{\sigma_i}{2}\phi_i^{x[1]}. \quad (101)$$

And from Eqs. (94) and (95), respectively, the $O(\varepsilon)$ equations are,

$$\frac{\psi_{t,i+1/2}^{[1]} - \psi_{t,i-1/2}^{[1]}}{\Delta\ell_{t,i}} + \sigma_i\psi_{t,i}^{[2]} = \frac{\sigma_i}{2}\phi_i^{[2]} - \frac{\sigma_{ai}}{2}\phi_i^{[0]} + \frac{1}{2}q_i, \quad (102)$$

and,

$$\frac{3[\psi_{t,i+1/2}^{[1]} + \psi_{t,i-1/2}^{[1]} - 2\psi_{t,i}^{[1]}]}{\Delta\ell_{t,i}} + \sigma_i\psi_{t,i}^{x[2]} = \frac{\sigma_i}{2}\phi_i^{x[2]} - \frac{\sigma_{ai}}{2}\phi_i^{x[0]} + \frac{1}{2}q_i^x. \quad (103)$$

We use previous work by Wareing [War 92] for guidance in how to manipulate these equations to construct a leading order scalar flux solution on the cell edges. We can operate on Eqs. (100) and (101) by multiplying by the volumetric weight and summing over all tubes:

$$\sum_t \frac{(\psi_{t,i+1/2}^{[0]} - \psi_{t,i-1/2}^{[0]})}{\Delta \ell_{t,i}} \Delta_{t,i} = 0 \quad (104)$$

$$\sum_t \frac{3(\psi_{t,i+1/2}^{[0]} + \psi_{t,i-1/2}^{[0]} - 2\psi_{t,i}^{[0]})}{\Delta \ell_{t,i}} \Delta_{t,i} = 0 \quad (105)$$

Eqs. (104) and (105) lead to the following relationship containing the leading order edge angular fluxes

$$\sum_t \psi_{t,i\pm 1/2}^{[0]} \frac{\Delta_{t,i}}{\Delta \ell_{t,i}} = 0. \quad (106)$$

Eqs. (98) and (99) are multiplied by the ratio of the volumetric weight to the average characteristic pathlength and summed over all tubes yielding,

$$(\phi_i^{[0]} + \phi_i^{x[0]}) = (\phi_{i+1}^{[0]} - \phi_{i+1}^{x[0]}) \equiv \phi_{i+1/2}^{[0]}, \quad (107)$$

and,

$$(\phi_{i-1}^{[0]} + \phi_{i-1}^{x[0]}) = (\phi_i^{[0]} - \phi_i^{x[0]}) \equiv \phi_{i-1/2}^{[0]}, \quad (108)$$

due to the symmetry of the space-angle mesh. Adding and subtracting Eqs. (107) and (108) leads to,

$$\phi_i^{[0]} = \frac{1}{2}(\phi_{i+1/2}^{[0]} + \phi_{i-1/2}^{[0]}), \quad (109)$$

and,

$$\phi_i^{x[0]} = \frac{1}{2}(\phi_{i+1/2}^{[0]} - \phi_{i-1/2}^{[0]}). \quad (110)$$

For all of the interior cells, the cell edge leading order angular flux is isotropic

$$\psi_{t,i\pm 1/2}^{[0]} = \frac{1}{2}\phi_{i\pm 1/2}^{[0]}. \quad (111)$$

Next, Eq. (100) is multiplied by the ratio of the volumetric weight to the average characteristic pathlength and summed over all tubes yielding,

$$\sum_t \frac{\psi_{t,i+1/2}^{[0]} - \psi_{t,i-1/2}^{[0]}}{\Delta\ell_{t,i}} \frac{\Delta_{t,i}}{\Delta\ell_{t,i}} + \sum_t \sigma_i \psi_{t,i}^{[1]} \frac{\Delta_{t,i}}{\Delta\ell_{t,i}} = \sum_t \frac{\sigma_i}{2} \phi_i^{[1]} \frac{\Delta_{t,i}}{\Delta\ell_{t,i}}. \quad (112)$$

For simplicity, we define the cell-centered current,

$$r_i^2 J_i^{[1]} \equiv \sum_t \psi_{t,i}^{[1]} \frac{\Delta_{t,i}}{\Delta\ell_{t,i}}, \quad (113)$$

which leads to the conditions:

$$r_i^2 J_i^{[1]} = -\frac{1}{2\sigma_i} (\phi_{i+1/2}^{[0]} - \phi_{i-1/2}^{[0]}) \sum_t \frac{\Delta_{t,i}}{\Delta\ell_{t,i}^2}, \quad 1 < i < I, \quad (114)$$

$$r_I^2 J_I^{[1]} = -\frac{1}{2\sigma_I} \left[\left(\frac{1}{2}\phi_{I+1/2}^{[0]} - \phi_{I-1/2}^{[0]} \right) \sum_t \frac{\Delta_{t,I}}{\Delta\ell_{t,I}^2} + 2 \sum_{\Delta\ell_{t,I}>0} g_t \frac{\Delta_{t,I}}{\Delta\ell_{t,I}^2} \right]. \quad (115)$$

Finally, we operate on Eqs. (102) and (103) by multiplying by the volumetric weight and summing over all tubes leading to the following cell-edge current equations:

$$r_{i+1/2}^2 J_{i+1/2}^{[1]} - r_{i-1/2}^2 J_{i-1/2}^{[1]} = -\sigma_{ai} \Delta V_i \phi_i^{[0]} + \Delta V_i q_i, \quad (116)$$

and,

$$r_{i+1/2}^2 J_{i+1/2}^{[1]} + r_{i-1/2}^2 J_{i-1/2}^{[1]} = 2r_i^2 J_i^{[1]} - \frac{1}{3} \sigma_{ai} \Delta V_i \phi_i^{[0]} + \frac{1}{3} \Delta V_i q_i. \quad (117)$$

By summing Eq. (116) for two adjacent cells and subtracting Eq. (117) for two adjacent cells we end up with the following current difference equations, respectively:

$$\begin{aligned} r_{i+3/2}^2 J_{i+3/2}^{[1]} - r_{i-1/2}^2 J_{i-1/2}^{[1]} &= -(\sigma_{ai} \Delta V_i \phi_i^{[0]} + \sigma_{ai+1} \Delta V_{i+1} \phi_{i+1}^{[0]}) \\ &+ (\Delta V_i q_i + \Delta V_{i+1} q_{i+1}), \end{aligned} \quad (118)$$

and,

$$\begin{aligned} r_{i+3/2}^2 J_{i+3/2}^{[1]} - r_{i-1/2}^2 J_{i-1/2}^{[1]} &= 2(r_{i+1}^2 J_{i+1}^{[1]} - r_i^2 J_i^{[1]}) \\ &- \frac{1}{3} (\sigma_{ai+1} \Delta V_{i+1} \phi_{i+1}^{x[0]} - \sigma_{ai} \Delta V_i \phi_i^{x[0]}) + \frac{1}{3} (\Delta V_{i+1} q_{i+1}^x - \Delta V_i q_i^x). \end{aligned} \quad (119)$$

By equating Eqs. (118) and (119) we obtain a discrete diffusion equation for the leading order scalar flux on the interior edges of the problem. This equation contains a three-point leakage term, and a three-point removal term:

$$\begin{aligned}
& -\frac{1}{2\sigma_{i+1}}(\phi_{i+3/2}^{[0]} - \phi_{i+1/2}^{[0]}) \sum_t \frac{\Delta_{t,i+1}}{\Delta \ell_{t,i+1}^2} + \frac{1}{2\sigma_i}(\phi_{i+1/2}^{[0]} - \phi_{i-1/2}^{[0]}) \sum_t \frac{\Delta_{t,i}}{\Delta \ell_{t,i}^2} \\
& + \frac{1}{4}[\sigma_{a_i} \Delta V_i (\frac{4}{3}\phi_{i+1/2}^{[0]} + \frac{2}{3}\phi_{i-1/2}^{[0]}) + \sigma_{a_{i+1}} \Delta V_{i+1} (\frac{4}{3}\phi_{i+1/2}^{[0]} + \frac{2}{3}\phi_{i+3/2}^{[0]})], \quad 1 \leq i < I. \\
& = \frac{1}{2}[\Delta V_i (q_i + \frac{1}{3}q_i^x) + \Delta V_{i+1} (q_{i+1} - \frac{1}{3}q_{i+1}^x)]
\end{aligned} \tag{120}$$

With the reflecting boundary at the origin, cell $i = 1$, we can set $J_{i-1/2}^{[1]} = 0$ for both Eqs. (116) and (117) and equate the resulting equations. This leads to,

$$-\frac{1}{2\sigma_1}(\phi_{3/2}^{[0]} - \phi_{1/2}^{[0]}) \sum_t \frac{\Delta_{t,1}}{\Delta \ell_{t,1}^2} + \frac{1}{4}\sigma_{a_1} \Delta V_1 (\frac{4}{3}\phi_{1/2}^{[0]} + \frac{2}{3}\phi_{3/2}^{[0]}) = \frac{1}{2}\Delta V_1 (q_1 + \frac{1}{3}q_1^x) \tag{121}$$

Lastly, the boundary condition at $r = R$ that constrains the leading order scalar flux in the interior of the optically thick and diffusive region is a Dirichlet condition. Using the boundary conditions described in Eq. (86) we have determined a similar boundary condition where:

$$\phi_{I+1/2}^{[0]} = \frac{4}{\rho_I} \sum_{\Delta \ell_{t,I} > 0} g_t \frac{\Delta_{t,I}}{\Delta \ell_{t,I}}, \tag{122}$$

where,

$$\rho_I = 2 \sum_{\Delta \ell_{t,I} > 0} \frac{\Delta_{t,I}}{\Delta \ell_{t,I}}. \tag{123}$$

Now we would like to write Eq. (120) in terms of a new variable, $\Phi_{i+1/2}$, such that it will hold for the interior cells as well as the exterior boundary cell. Using Eqs. (115) and (122) we find that the solution is,

$$\begin{aligned}
& -\frac{1}{2\sigma_{i+1}}(\Phi_{i+3/2} - \Phi_{i+1/2}) \sum_t \frac{\Delta_{t,i+1}}{\Delta \ell_{t,i+1}^2} + \frac{1}{2\sigma_i}(\Phi_{i+1/2} - \Phi_{i-1/2}) \sum_t \frac{\Delta_{t,i}}{\Delta \ell_{t,i}^2} \\
& + \frac{1}{4}[\sigma_{ai}\Delta V_i(\frac{4}{3}\Phi_{i+1/2} + \frac{2}{3}\Phi_{i-1/2}) + \sigma_{ai+1}\Delta V_{i+1}(\frac{4}{3}\Phi_{i+1/2} + \frac{2}{3}\Phi_{i+3/2})], \quad 1 \leq i \leq I, \\
& = \frac{1}{2}[\Delta V_i(q_i + \frac{1}{3}q_i^x) + \Delta V_{i+1}(q_{i+1} - \frac{1}{3}q_{i+1}^x)]
\end{aligned} \tag{124}$$

and

$$\Phi_{i+1/2} = \phi_{i+1/2}^{[0]}, \quad 1 \leq i < I, \tag{125}$$

$$\frac{1}{2}\Phi_{I+1/2} = \frac{1}{\gamma_I - \alpha_I} \sum_{\Delta \ell_{t,I} > 0} \left[(\gamma_I - 2\alpha_I) \frac{\Delta \ell_{t,I}^{-1}}{\rho_I} + \frac{3\Delta \ell_{t,I}^{-2}}{2} \right] g_t \Delta_{t,I}, \tag{126}$$

where,

$$\gamma_I = \frac{3}{2} \sum_t \frac{\Delta_{t,I}}{\Delta \ell_{t,I}^2} \tag{127}$$

$$\alpha_I = \frac{1}{2} \sigma_I \sigma_{aI} \Delta V_I$$

The results in Eqs. (120), (121), and (122) are a reasonable discretization of the diffusion equation with accurate boundary conditions in Eq. (126). The 3-point removal term can contribute to unphysical oscillations in the solution. However, this analysis predicts that the LCMOT method is well behaved in thick and diffusive regions.

5 DIFFUSION SYNTHETIC ACCELERATION OF LCMOT

5.1 Introduction

In this chapter, we derive a Diffusion Synthetic Acceleration (DSA) scheme for the efficient iterative solution of the LCMOT transport equations. Here, the fact that the diffusion limit for the slab geometry linear characteristic and the slab geometry linear discontinuous is equivalent, the assumption is made that the DSA scheme will be equivalent for the LCMOT and a linear discontinuous Method of Tubes (LDMOT) under the assumption that the diffusion limit for the LDMOT and LCMOT schemes are the same. The DSA scheme is derived from an LDMOT discretization.

5.2 Linear Discontinuous Method of Tubes (LDMOT)

Finite Element Methods (FEM's) are derived by approximating the solution as a fixed shape. Given, the number of degrees of freedom for the solution shape, I , we must take I weighted residuals of the governing equations to fully define the FEM. We define the basis functions for LDMOT that approximate the solution as linear in the ℓ coordinate:

$$\psi(\ell) = \psi_L b_L(\ell) + \psi_R b_R(\ell), \quad Q(\ell) = Q_L b_L(\ell) + Q_R b_R(\ell), \quad (128)$$

$$b_R(\ell) = \frac{\ell - \ell_{t,i-1/2}}{\Delta\ell_{t,i}}, \quad b_L(\ell) = \frac{\ell_{t,i+1/2} - \ell}{\Delta\ell_{t,i}}. \quad (129)$$

Notice that by substituting the basis function expansions of the solution and source into our governing transport equation, we will have only a single equation

for two unknowns (ψ_{Li} and ψ_{Ri}) for each cell. We multiply the governing equations by two weighting functions that span the same functional space as the chosen linear basis functions. Then we integrate the two weighted residual equations over a cell to define all unknowns:

$$\int_{\ell_{t,i-1/2}}^{\ell_{t,i+1/2}} w_j(\ell) \left[\frac{\partial \psi(\ell)}{\partial \ell} + \sigma_i \psi(\ell) \right] d\ell = \frac{1}{2} \int_{\ell_{t,i-1/2}}^{\ell_{t,i+1/2}} w_j(\ell) Q(\ell) d\ell, \quad (130)$$

where,

$$w_1(\ell) = \frac{\ell - \ell_{t,i-1/2}}{\Delta \ell_{t,i}}, \quad w_2(\ell) = \frac{\ell_{t,i+1/2} - \ell}{\Delta \ell_{t,i}}. \quad (131)$$

Evaluating Eq. (130) for both weighting functions and substituting the basis function expansions (Eq. (128)) when necessary, we obtain the LDMOT discretized equations:

$$\begin{aligned} & \left[\frac{\psi_{t,Li}^{(l+1/2)} + \psi_{t,Ri}^{(l+1/2)}}{2} - \psi_{t,i-1/2}^{(l+1/2)} \right] + \sigma_i \Delta \ell_{t,i} \left[\frac{\psi_{t,Li}^{(l+1/2)}}{3} + \frac{\psi_{t,Ri}^{(l+1/2)}}{6} \right] \\ & = \Delta \ell_{t,i} \left[\frac{Q_{t,Li}^{(l)}}{3} + \frac{Q_{t,Ri}^{(l)}}{6} \right], \end{aligned} \quad (132)$$

$$\begin{aligned} & \left[\psi_{t,i+1/2}^{(l+1/2)} - \frac{\psi_{t,Li}^{(l+1/2)} + \psi_{t,Ri}^{(l+1/2)}}{2} \right] + \sigma_i \Delta \ell_{t,i} \left[\frac{\psi_{t,Li}^{(l+1/2)}}{6} + \frac{\psi_{t,Ri}^{(l+1/2)}}{3} \right] \\ & = \Delta \ell_{t,i} \left[\frac{Q_{t,Li}^{(l)}}{6} + \frac{Q_{t,Ri}^{(l)}}{3} \right], \end{aligned} \quad (133)$$

where the closure for cell-edge angular fluxes is,

$$\psi_{t,i-1/2} = \begin{cases} \psi_t^*, & \mu_t > 0, \quad i = 1, \\ \psi_{t,Li}, & \mu_t < 0, \quad 1 < i \leq I, \end{cases} \quad (134)$$

$$\psi_{t,i+1/2} = \begin{cases} \psi_{t,inc}, & \mu_t < 0, \quad i = I, \\ \psi_{t,Ri}, & \mu_t > 0, \quad 1 \leq i < I. \end{cases} \quad (135)$$

The ψ_t^* is known due to the reflecting boundary conditions in each of the tubes at $\mu = 0$. The source on the right-hand-side of the Eqs. (132) and (133) is defined by,

$$Q_t^{(l)}(r) = \frac{1}{2}(\sigma_s(r)\phi^{(l)}(r) + q(r)). \quad (136)$$

After a transport sweep has been completed we can define “corrections”, that if available, would yield the converged solution to the transport problem:

$$f_t(r) = \psi_t^{\text{converged}}(r) - \psi_t^{(l+1/2)}(r), \quad (137)$$

$$F_t(r) = \phi_t^{\text{converged}}(r) - \phi_t^{(l+1/2)}(r). \quad (138)$$

We generate exact equations for these corrections by subtracting the iteration equations (Eqs. (132-135)) from the converged equations:

$$\begin{aligned} & \left[\frac{f_{t,Li} + f_{t,Ri}}{2} - f_{t,i-1/2} \right] + \sigma_i \Delta \ell_{t,i} \left[\frac{f_{t,Li}}{3} + \frac{f_{t,Ri}}{6} \right] - \frac{\sigma_{si} \Delta \ell_{t,i}}{2} \left[\frac{F_{Li}}{3} + \frac{F_{Ri}}{6} \right] \\ & = \frac{\sigma_{si} \Delta \ell_{t,i}}{2} \left[\frac{\phi_{Li}^{(l+1/2)} - \phi_{Li}^{(l)}}{3} + \frac{\phi_{Ri}^{(l+1/2)} - \phi_{Ri}^{(l)}}{6} \right], \end{aligned} \quad (139)$$

$$\begin{aligned}
& \left[f_{t,i+1/2} - \frac{f_{t,Li} + f_{t,Ri}}{2} \right] + \sigma_i \Delta \ell_{t,i} \left[\frac{f_{t,Li}}{6} + \frac{f_{t,Ri}}{3} \right] - \frac{\sigma_{si} \Delta \ell_{t,i}}{2} \left[\frac{F_{Li}}{6} + \frac{F_{Ri}}{3} \right] \\
& = \frac{\sigma_{si} \Delta \ell_{t,i}}{2} \left[\frac{\phi_{Li}^{(l+1/2)} - \phi_{Li}^{(l)}}{6} + \frac{\phi_{Ri}^{(l+1/2)} - \phi_{Ri}^{(l)}}{3} \right], \tag{140}
\end{aligned}$$

$$f_{t,i-1/2} = \begin{cases} f_t^*, & \mu_t > 0, \quad i = 1, \\ f_{t,Li}, & \mu_t < 0, \quad 1 < i \leq I, \end{cases} \tag{141}$$

$$f_{t,i+1/2} = \begin{cases} f_{t,inc}, & \mu_t < 0, \quad i = I, \\ f_{t,Ri}, & \mu_t > 0, \quad 1 \leq i < I. \end{cases} \tag{142}$$

5.3 Modified Four-Step

For this particular derivation of DSA we will follow the Modified Four-Step (M4S) procedure [Ada 02]. The M4S procedure is as follows:

A. Calculate the zero-th and first angular moments of the discretized transport equation for LDMOT.

B. Change the iteration indices to $l + 1$, except on the second and higher moment terms to obtain acceleration equations.

C. Subtract the acceleration equations from the unaccelerated equations to reduce algebraic complexity.

D. Eliminate the first angular flux moments from the resulting system, leaving discretized diffusion equations for the scalar fluxes.

Step (A) of the M4S procedure involves taking the zero-th angular moment of the transport equations. To do this, we first operate on Eqs. (139) and (140) by multiplying the equations by the volumetric weight of a cell and summing over the tubes yielding,

$$\begin{aligned}
& \sum_t \left[\frac{f_{t,Li} + f_{t,Ri}}{2} - f_{t,i-1/2} \right] \frac{\Delta_{t,i}}{\Delta \ell_{t,i}} + \sigma_{ai} \Delta V_i \left[\frac{F_{Li}}{3} + \frac{F_{Ri}}{6} \right] \\
& = \sigma_{si} \Delta V_i \left[\frac{\phi_{Li}^{(l+1/2)} - \phi_{Li}^{(l)}}{3} + \frac{\phi_{Ri}^{(l+1/2)} - \phi_{Ri}^{(l)}}{6} \right], \tag{143}
\end{aligned}$$

$$\begin{aligned}
& \sum_t \left[f_{t,i+1/2} - \frac{f_{t,Li} + f_{t,Ri}}{2} \right] \frac{\Delta_{t,i}}{\Delta \ell_{t,i}} + \sigma_{ai} \Delta V_i \left[\frac{F_{Li}}{6} + \frac{F_{Ri}}{3} \right] \\
& = \sigma_{si} \Delta V_i \left[\frac{\phi_{Li}^{(l+1/2)} - \phi_{Li}^{(l)}}{6} + \frac{\phi_{Ri}^{(l+1/2)} - \phi_{Ri}^{(l)}}{3} \right]. \tag{144}
\end{aligned}$$

We will now take the first angular moment of the correction equations by multiplying Eqs. (139) and (140) by the volumetric weight and angle and summing over all tubes:

$$\sum_t \left[\frac{f_{t,Li} + f_{t,Ri}}{2} - f_{t,i-1/2} \right] \frac{\Delta_{t,i}}{\Delta \ell_{t,i}^2} + \sigma_i \sum_t \left[\frac{f_{t,Li}}{3} + \frac{f_{t,Ri}}{6} \right] \frac{\Delta_{t,i}}{\Delta \ell_{t,i}} = 0, \tag{145}$$

$$\sum_t \left[f_{t,i+1/2} - \frac{f_{t,Li} + f_{t,Ri}}{2} \right] \frac{\Delta_{t,i}}{\Delta \ell_{t,i}^2} + \sigma_i \sum_t \left[\frac{f_{t,Li}}{6} + \frac{f_{t,Ri}}{3} \right] \frac{\Delta_{t,i}}{\Delta \ell_{t,i}} = 0. \tag{146}$$

Equations (145) and (146) are simplified utilizing the symmetry of the space-angle mesh:

$$\sum_t \frac{\Delta_{t,i}}{\Delta \ell_{t,i}} = 0. \tag{147}$$

At this point we made no approximation in these derivations. Therefore, it is just as difficult to solve this problem as it is to perform the source iteration

transport sweeps. Here we will introduce the P_1 approximation. This is defined as the truncated P_1 angular flux expansion:

$$f_t(r) = \frac{1}{2}(F(r) + 3\mu_t(r)G(r)), \quad (148)$$

where $G(r)$ is defined as the net current at a position r . We use this approximation to simplify the first term on the left-hand-side of Eqs. (145) and (146). This leads to the following relationships:

$$\frac{1}{2} \left[\frac{F_{Li} + F_{Ri}}{2} - F_{i-1/2} \right] \sum_t \frac{\Delta_{t,i}}{\Delta \ell_{t,i}^2} + \sigma_i \sum_t \left[\frac{f_{t,Li}}{3} + \frac{f_{t,Ri}}{6} \right] \frac{\Delta_{t,i}}{\Delta \ell_{t,i}} = 0, \quad (149)$$

$$\frac{1}{2} \left[F_{i+1/2} - \frac{F_{Li} + F_{Ri}}{2} \right] \sum_t \frac{\Delta_{t,i}}{\Delta \ell_{t,i}^2} + \sigma_i \sum_t \left[\frac{f_{t,Li}}{6} + \frac{f_{t,Ri}}{3} \right] \frac{\Delta_{t,i}}{\Delta \ell_{t,i}} = 0. \quad (150)$$

Up to this point we have performed the exact steps associated with the original four-step procedure [Lar 82]. Instead of operating on the closure conditions in Eqs. (141) and (142) we use an approximate closure for the scalar fluxes. The significant difference in the M4S procedure is shown in the closure approximation:

$$F_{i-1/2} = F_{Li}, \quad (151)$$

$$F_{i+1/2} = F_{Ri}. \quad (152)$$

With these definitions, Eqs. (149) and (150) now become:

$$-\frac{1}{4\sigma_i} [F_{Ri} - F_{Li}] \sum_t \frac{\Delta_{t,i}}{\Delta \ell_{t,i}^2} = \sum_t \left[\frac{f_{t,Li}}{3} + \frac{f_{t,Ri}}{6} \right] \frac{\Delta_{t,i}}{\Delta \ell_{t,i}}, \quad (153)$$

$$-\frac{1}{4\sigma_i} [F_{Ri} - F_{Li}] \sum_t \frac{\Delta_{t,i}}{\Delta \ell_{t,i}^2} = \sum_t \left[\frac{f_{t,Li}}{6} + \frac{f_{t,Ri}}{3} \right] \frac{\Delta_{t,i}}{\Delta \ell_{t,i}}. \quad (154)$$

Eqs. (153) and (154) imply,

$$\sum_t f_{t,Li} \frac{\Delta_{t,i}}{\Delta \ell_{t,i}} = \sum_t f_{t,Ri} \frac{\Delta_{t,i}}{\Delta \ell_{t,i}} = -\frac{1}{2\sigma_i} [F_{Ri} - F_{Li}] \sum_t \frac{\Delta_{t,i}}{\Delta \ell_{t,i}^2}. \quad (155)$$

Also, we can determine the current values, G_{Li} and G_{Ri} , by substituting the P_1 expansion in Eq. (148) into Eq. (155) with the result shown below:

$$G_{Li} = -\frac{1}{3\sigma_i} [F_{Ri} - F_{Li}] \frac{\sum_t \frac{\Delta_{t,i}}{\Delta \ell_{t,i}^2}}{\sum_t \frac{\mu_{t,i-1/2} \Delta_{t,i}}{\Delta \ell_{t,i}}}, \quad (156)$$

$$G_{Ri} = -\frac{1}{3\sigma_i} [F_{Ri} - F_{Li}] \frac{\sum_t \frac{\Delta_{t,i}}{\Delta \ell_{t,i}^2}}{\sum_t \frac{\mu_{t,i+1/2} \Delta_{t,i}}{\Delta \ell_{t,i}}}. \quad (157)$$

Lastly, we make use of the closure equations (Eqs. (141) and (142)) to determine the final unknown terms in Eqs. (143) and (144). We multiply the closure equations by the ratio of the the volumetric weight to the average characteristic length and sum over all tubes yielding,

$$\sum_t f_{t,i+1/2} \frac{\Delta_{t,i}}{\Delta \ell_{t,i}} = \sum_{\Delta \ell_{t,i} > 0} f_{t,Ri} \frac{\Delta_{t,i}}{\Delta \ell_{t,i}} + \sum_{\Delta \ell_{t,i} < 0} f_{t,Li+1} \frac{\Delta_{t,i}}{\Delta \ell_{t,i}}, \quad (158)$$

$$\sum_t f_{t,i-1/2} \frac{\Delta_{t,i}}{\Delta \ell_{t,i}} = \sum_{\Delta \ell_{t,i} > 0} f_{t,Ri-1} \frac{\Delta_{t,i}}{\Delta \ell_{t,i}} + \sum_{\Delta \ell_{t,i} < 0} f_{t,Li} \frac{\Delta_{t,i}}{\Delta \ell_{t,i}}. \quad (159)$$

We substitute the P_1 expansion into the angular flux correction terms on the right-hand-side of Eqs. (158) and (159) leading to:

$$\begin{aligned}
\sum_t f_{t,i+1/2} \frac{\Delta_{t,i}}{\Delta \ell_{t,i}} &= \frac{1}{2} (F_{Ri} - F_{Li+1}) \sum_{\Delta \ell_{t,i} > 0} \frac{\Delta_{t,i}}{\Delta \ell_{t,i}} \\
&- \frac{1}{2\sigma_i} \left[(F_{Ri} - F_{Li}) \frac{\sum_t \frac{\Delta_{t,i}}{\Delta \ell_{t,i}^2}}{\sum_t \frac{\mu_{t,i+1/2} \Delta_{t,i}}{\Delta \ell_{t,i}}} \right] \sum_{\Delta \ell_{t,i} > 0} \frac{\mu_{t,i+1/2} \Delta_{t,i}}{\Delta \ell_{t,i}} \\
&- \frac{1}{2\sigma_{i+1}} \left[(F_{Ri+1} - F_{Li+1}) \frac{\sum_t \frac{\Delta_{t,i+1}}{\Delta \ell_{t,i+1}^2}}{\sum_t \frac{\mu_{t,i+1/2} \Delta_{t,i+1}}{\Delta \ell_{t,i+1}}} \right] \sum_{\Delta \ell_{t,i} > 0} \frac{\mu_{t,i+1/2} \Delta_{t,i}}{\Delta \ell_{t,i}},
\end{aligned} \tag{160}$$

$$\begin{aligned}
\sum_t f_{t,i-1/2} \frac{\Delta_{t,i}}{\Delta \ell_{t,i}} &= \frac{1}{2} (F_{Ri-1} - F_{Li}) \sum_{\Delta \ell_{t,i} > 0} \frac{\Delta_{t,i}}{\Delta \ell_{t,i}} \\
&- \frac{1}{2\sigma_{i-1}} \left[(F_{Ri-1} - F_{Li-1}) \frac{\sum_t \frac{\Delta_{t,i-1}}{\Delta \ell_{t,i-1}^2}}{\sum_t \frac{\mu_{t,i-1/2} \Delta_{t,i-1}}{\Delta \ell_{t,i-1}}} \right] \sum_{\Delta \ell_{t,i} > 0} \frac{\mu_{t,i-1/2} \Delta_{t,i}}{\Delta \ell_{t,i}} \\
&- \frac{1}{2\sigma_i} \left[(F_{Ri} - F_{Li}) \frac{\sum_t \frac{\Delta_{t,i}}{\Delta \ell_{t,i}^2}}{\sum_t \frac{\mu_{t,i-1/2} \Delta_{t,i}}{\Delta \ell_{t,i}}} \right] \sum_{\Delta \ell_{t,i} > 0} \frac{\mu_{t,i-1/2} \Delta_{t,i}}{\Delta \ell_{t,i}}.
\end{aligned} \tag{161}$$

By substituting Eqs. (155), (160), and (161) into Eqs. (143) and (144) we obtain a diffusion equation scheme for the interior cells:

$$\begin{aligned}
& \left[\frac{1}{2\sigma_i} \sum_t \frac{\Delta_{t,i}}{\Delta \ell_{t,i}^2} \left(1 - \frac{\sum_{\Delta \ell_{t,i} > 0} \frac{\mu_{t,i-1/2} \Delta_{t,i}}{\Delta \ell_{t,i}}}{\sum_t \frac{\mu_{t,i-1/2} \Delta_{t,i}}{\Delta \ell_{t,i}}} \right) + \frac{1}{2} \sum_{\Delta \ell_{t,i} > 0} \frac{\Delta_{t,i}}{\Delta \ell_{t,i}} + \frac{1}{3} \sigma_{ai} \Delta V_i \right] F_{Li} \\
& + \left[\frac{1}{2\sigma_i} \sum_t \frac{\Delta_{t,i}}{\Delta \ell_{t,i}^2} \left(\frac{\sum_{\Delta \ell_{t,i} > 0} \frac{\mu_{t,i-1/2} \Delta_{t,i}}{\Delta \ell_{t,i}}}{\sum_t \frac{\mu_{t,i-1/2} \Delta_{t,i}}{\Delta \ell_{t,i}}} - 1 \right) + \frac{1}{6} \sigma_{ai} \Delta V_i \right] F_{Ri} \\
& + \left[\frac{1}{2\sigma_{i-1}} \sum_t \frac{\Delta_{t,i-1}}{\Delta \ell_{t,i-1}^2} \left(\frac{\sum_{\Delta \ell_{t,i} > 0} \frac{\mu_{t,i-1/2} \Delta_{t,i}}{\Delta \ell_{t,i}}}{\sum_t \frac{\mu_{t,i-1/2} \Delta_{t,i-1}}{\Delta \ell_{t,i-1}}} \right) - \frac{1}{2} \sum_{\Delta \ell_{t,i} > 0} \frac{\Delta_{t,i}}{\Delta \ell_{t,i}} \right] F_{Ri-1} \\
& + \left[-\frac{1}{2\sigma_{i-1}} \sum_t \frac{\Delta_{t,i-1}}{\Delta \ell_{t,i-1}^2} \left(\frac{\sum_{\Delta \ell_{t,i} > 0} \frac{\mu_{t,i-1/2} \Delta_{t,i}}{\Delta \ell_{t,i}}}{\sum_t \frac{\mu_{t,i-1/2} \Delta_{t,i-1}}{\Delta \ell_{t,i-1}}} \right) \right] F_{Li-1} \\
& = \sigma_{si} \Delta V_i \left[\frac{\phi_i^{(l+1/2)} - \phi_i^{(l)}}{2} - \frac{\phi_i^{x(l+1/2)} - \phi_i^{x(l)}}{6} \right], \quad 1 < i \leq I,
\end{aligned} \tag{162}$$

$$\begin{aligned}
& \left[\frac{1}{2\sigma_i} \sum_t \frac{\Delta_{t,i}}{\Delta \ell_{t,i}^2} \left(1 - \frac{\sum_{\Delta \ell_{t,i} > 0} \frac{\mu_{t,i+1/2} \Delta_{t,i}}{\Delta \ell_{t,i}}}{\sum_t \frac{\mu_{t,i+1/2} \Delta_{t,i}}{\Delta \ell_{t,i}}} \right) + \frac{1}{2} \sum_{\Delta \ell_{t,i} > 0} \frac{\Delta_{t,i}}{\Delta \ell_{t,i}} + \frac{1}{3} \sigma_{ai} \Delta V_i \right] F_{Ri} \\
& + \left[\frac{1}{2\sigma_i} \sum_t \frac{\Delta_{t,i}}{\Delta \ell_{t,i}^2} \left(\frac{\sum_{\Delta \ell_{t,i} > 0} \frac{\mu_{t,i+1/2} \Delta_{t,i}}{\Delta \ell_{t,i}}}{\sum_t \frac{\mu_{t,i+1/2} \Delta_{t,i}}{\Delta \ell_{t,i}}} - 1 \right) + \frac{1}{6} \sigma_{ai} \Delta V_i \right] F_{Li} \\
& + \left[\frac{1}{2\sigma_{i+1}} \sum_t \frac{\Delta_{t,i+1}}{\Delta \ell_{t,i+1}^2} \left(\frac{\sum_{\Delta \ell_{t,i+1} > 0} \frac{\mu_{t,i+1/2} \Delta_{t,i+1}}{\Delta \ell_{t,i+1}}}{\sum_t \frac{\mu_{t,i+1/2} \Delta_{t,i+1}}{\Delta \ell_{t,i+1}}} \right) - \frac{1}{2} \sum_{\Delta \ell_{t,i+1} > 0} \frac{\Delta_{t,i+1}}{\Delta \ell_{t,i+1}} \right] F_{Li+1} \\
& + \left[-\frac{1}{2\sigma_{i+1}} \sum_t \frac{\Delta_{t,i+1}}{\Delta \ell_{t,i+1}^2} \left(\frac{\sum_{\Delta \ell_{t,i+1} > 0} \frac{\mu_{t,i+1/2} \Delta_{t,i+1}}{\Delta \ell_{t,i+1}}}{\sum_t \frac{\mu_{t,i+1/2} \Delta_{t,i+1}}{\Delta \ell_{t,i+1}}} \right) \right] F_{Ri+1} \\
& = \sigma_{si} \Delta V_i \left[\frac{\phi_i^{(l+1/2)} - \phi_i^{(l)}}{2} + \frac{\phi_i^{x(l+1/2)} - \phi_i^{x(l)}}{6} \right], \quad 1 \leq i < I.
\end{aligned} \tag{163}$$

The source on the right-hand-side of Eqs. (162) and (163) has been written in terms of average-slope knowns instead of left-right knowns.

At this point we have $2(I-1)$ equations for $2I$ unknowns. We need an equation for the outer boundary condition and we need an equation for the inner reflecting boundary. First, we apply the reflecting inner boundary condition with:

$$\sum_t f_{t,1/2} \frac{\Delta_{t,1}}{\Delta \ell_{t,1}} = 0. \tag{164}$$

This definition and Eq. (155), for $i = 1$, are used with Eq. (143) to obtain:

$$\begin{aligned}
& \left[\frac{1}{2\sigma_1} \sum_t \frac{\Delta_{t,1}}{\Delta \ell_{t,1}^2} + \frac{1}{3} \sigma_{a1} \Delta V_i \right] F_{L1} + \left[\frac{1}{2\sigma_1} \sum_t \frac{\Delta_{t,1}}{\Delta \ell_{t,1}^2} + \frac{1}{6} \sigma_{a1} \Delta V_1 \right] F_{R1} \\
& = \sigma_{s1} \Delta V_1 \left[\frac{\phi_1^{(l+1/2)} - \phi_1^{(l)}}{2} - \frac{\phi_1^{x(l+1/2)} - \phi_1^{x(l)}}{6} \right].
\end{aligned} \tag{165}$$

We use the outer boundary condition in Eq. (142) and formulate an equation similar to Eq. (158) for the outermost cell:

$$\sum_t f_{t,I+1/2} \frac{\Delta_{t,I}}{\Delta \ell_{t,I}} = \sum_{\Delta \ell_{t,I} > 0} f_{t,RI} \frac{\Delta_{t,I}}{\Delta \ell_{t,I}} + \sum_{\Delta \ell_{t,I} < 0} f_{t,inc} \frac{\Delta_{t,I}}{\Delta \ell_{t,I}}. \tag{166}$$

This leads to:

$$\begin{aligned}
\sum_t f_{t,I+1/2} \frac{\Delta_{t,I}}{\Delta \ell_{t,I}} & = \frac{1}{2} F_{RI} \sum_{\Delta \ell_{t,I} > 0} \frac{\Delta_{t,I}}{\Delta \ell_{t,I}} - \sum_{\Delta \ell_{t,I} > 0} f_{t,inc} \frac{\Delta_{t,I}}{\Delta \ell_{t,I}} \\
& - \frac{1}{2\sigma_I} \left[(F_{RI} - F_{LI}) \frac{\sum_t \frac{\Delta_{t,I}}{\Delta \ell_{t,I}^2}}{\sum_t \frac{\mu_{t,I+1/2} \Delta_{t,I}}{\Delta \ell_{t,I}}} \right] \sum_{\Delta \ell_{t,I} > 0} \frac{\mu_{t,I+1/2} \Delta_{t,I}}{\Delta \ell_{t,I}}.
\end{aligned} \tag{167}$$

We substitute Eq. (167) and Eq. (155), for $i = I$, into Eq. (144) and obtain:

$$\begin{aligned}
& \left[\frac{1}{2\sigma_I} \sum_t \frac{\Delta_{t,I}}{\Delta \ell_{t,I}^2} \left(1 - \frac{\sum_{\Delta \ell_{t,I} > 0} \frac{\mu_{t,I+1/2} \Delta_{t,I}}{\Delta \ell_{t,I}}}{\sum_t \frac{\mu_{t,I+1/2} \Delta_{t,I}}{\Delta \ell_{t,I}}} \right) + \frac{1}{2} \sum_{\Delta \ell_{t,I} > 0} \frac{\Delta_{t,I}}{\Delta \ell_{t,I}} + \frac{1}{3} \sigma_{aI} \Delta V_I \right] F_{RI} \\
& + \left[\frac{1}{2\sigma_I} \sum_t \frac{\Delta_{t,I}}{\Delta \ell_{t,I}^2} \left(\frac{\sum_{\Delta \ell_{t,I} > 0} \frac{\mu_{t,I+1/2} \Delta_{t,I}}{\Delta \ell_{t,I}}}{\sum_t \frac{\mu_{t,I+1/2} \Delta_{t,I}}{\Delta \ell_{t,I}}} - 1 \right) + \frac{1}{6} \sigma_{aI} \Delta V_I \right] F_{LI} \\
& = \sigma_{sI} \Delta V_I \left[\frac{\phi_I^{(l+1/2)} - \phi_I^{(l)}}{2} + \frac{\phi_I^{x(l+1/2)} - \phi_I^{x(l)}}{6} \right].
\end{aligned} \tag{168}$$

This linear system of equations is solved using a banded matrix solver to determine scalar fluxes updates. The $2I$ equations for all of the $2I$ unknowns are fully defined in Eqs. (162), (163), (165), and (168).

6 RESULTS

6.1 Introduction

In this chapter we present the results of several test problems that investigate the performance of our four versions of the MOT. We have used source iteration to solve the problems. We start with a guess for the source on the right-hand-side of the discretized transport equation. The scalar flux is obtained by sweeping over the space-angle mesh in Fig. 2. This calculated scalar flux is used for the source on the next iteration. We calculate the $L_2^{(l)}$ norm of the difference between the scalar flux solutions from two consecutive iterations,

$$L_2^{(l)} = \frac{\sqrt{\sum_i \left[\left(\phi_i^{(l)} - \phi_i^{(l-1)} \right) * \Delta r_i \right]^2}}{R}, \quad (169)$$

and if this value is sufficiently small, we determine that the solution is converged. We must be careful and protect against false convergence. This is absolutely necessary for optically thick and diffusive problems. To protect against false convergence we calculate the estimate of the spectral radius, which is just a ratio of two consecutive L_2 norms,

$$\rho^{(l)} = \frac{L_2^{(l)}}{L_2^{(l-1)}}. \quad (170)$$

The convergence criterion, E , is adjusted to account for slow convergence by,

$$E^* = E(1 - \rho^{(l)}). \quad (171)$$

To obtain an accurate solution to these test problems we continue iterating until the $L_2^{(l)}$ norm reaches E^* , which ensures a true relative error of E .

6.2 Test Problems

We have investigated the behavior of the four MOT schemes on several test problems: the Reed problem, a simple diffusion limit problem, a diffusion limit with an unresolved boundary layer, and a sequence of problems that demonstrate the rate of convergence of the transport solution to the asymptotic diffusion solution. For all of the test problems, we have chosen our convergence criteria to be $E = 10^{-6}$.

6.2.1 Reed Test Problem

The spherical geometry version of the Reed problem [Ree 71] is a good test of a transport method because it involves spatial regions with a variety of different transport physics: a thick absorber with a source, a thin absorber, a void region, a thin scatterer with a source and, and a source-free thin scatterer. Table 1 contains the Reed test problem definitions. We run this problem as a way of testing the implementation of the transport methods. The result from each method is compared against a “fully-lumped” LD solution [Pal 91].

Region	Spatial Interval	# of Intervals	σ_t	σ_s	q
1	$0 < r < 2$	10	50	0	50
2	$2 < r < 3$	5	5	0	0
3	$3 < r < 5$	10	0	0	0
4	$5 < r < 6$	5	1	0.9	0.7
5	$6 < r < 8$	10	1	0.9	0

Table 1: Test Problem 1

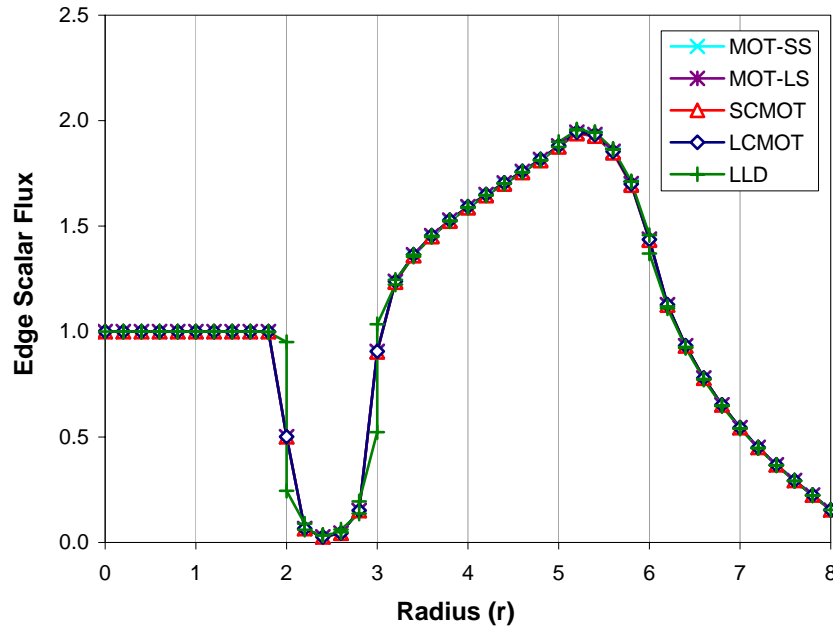


Figure 4: Problem 1 Solutions for all MOT Schemes and a “Fully-Lumped” LD Scheme.

Figure 4 shows that all MOT schemes yield nearly the same result using the same spatial mesh. Note that the Reed problem does not include any optically thick and diffusive regions.

6.2.2 A Test with a Diffusion Region

Here, we consider a two-region sphere with a vacuum outer boundary ($R = 20$) [Lar 90]: a central region with a source surrounded by an optically thick, purely scattering region. The spatial mesh is uniform and has 20 cells. The definitions for this test problem are shown in Table 2.

The exact solution in the central region is constant,

Region	Spatial Interval	# of Intervals	σ_t	σ_s	q
1	$0 < r < 10$	10	100	90	10
2	$10 < r < 20$	10	100	100	0

Table 2: Test Problem 2

$$\phi(r) = \frac{q}{\sigma_a} = 1, \quad (172)$$

and the interior of the outer region, the transport scalar flux approaches,

$$\phi(r) = 20 \phi(10) \left(\frac{1}{r} - \frac{1}{20} \right). \quad (173)$$

This exact solution is plotted with the numerical results for comparison in Fig. 5.

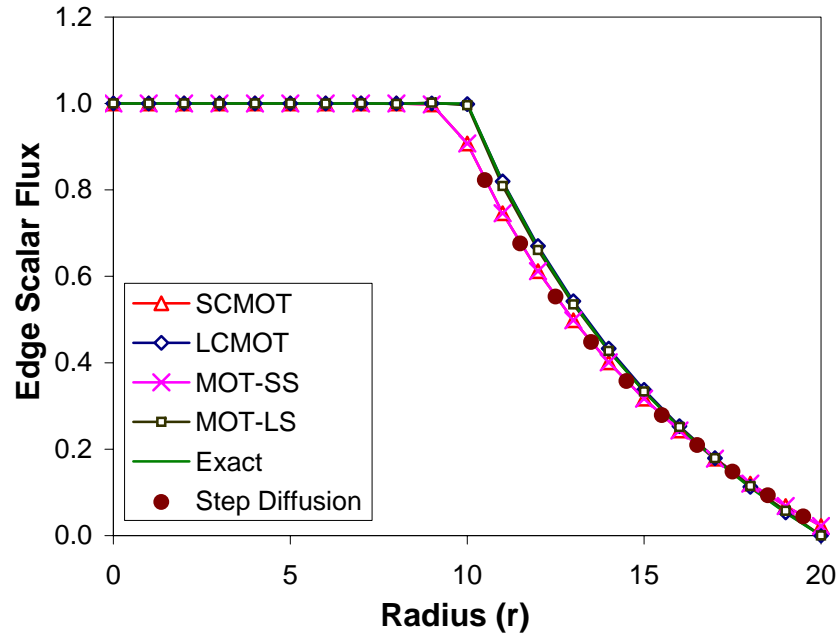


Figure 5: Problem 2 Solutions for all MOT Schemes.

Figure 5 illustrates the solution of this problem for all of the MOT schemes. Both of the moment-based versions of the MOT yield the correct solution in the

central region, and the correct shape in the outer region. Notice that the SCMOT solution at the interface between the two regions is significantly less accurate than the LCMOT solution. Also, both of the original methods (MOT-SS and MOT-LS) yield relatively accurate results as well.

Making use of the DSA scheme derived for LCMOT demonstrates how much faster the solutions can be obtained. Table 3 shows the differences in both the spectral radius and the number of iterations required to converge the solution.

Problem	Iterations	
	w/o DSA	w/ DSA
2	3503419	7

Table 3: SI vs. DSA for LCMOT

6.2.3 A Diffusion Test with an Unresolved Boundary Layer

This problem involves a source-free, two-region sphere ($R = 11$) subjected to an isotropic incident angular flux $\psi(R, \mu)=1$ on the outer boundary. The central region is a thick, pure scatterer ($\sigma_t=\sigma_s=100$), and the outer region is a relatively thin pure absorber ($\sigma_t=2$) [Lar 90]. The problem is solved with a spatial mesh containing 10 uniform cells in each region. Table 4 shows the definitions for this test problem.

Region	Spatial Interval	# of Intervals	σ_t	σ_s	q
1	$0 < r < 10$	10	100	100	0
2	$10 < r < 11$	10	2	0	0

Table 4: Test Problem 3

The flux incident on the sphere (at $r=11$) is attenuated in the outer pure

Region	Spatial Interval	# of Intervals	σ_t	σ_s	q
1	$0 < r < 10$	10	100	100	0
2	$10 < r < 11$	10	4	0	0

Table 5: Test Problem 3'

absorbing region to create an anisotropic angular flux coming into the central diffusion region (at $r=10$). This incoming angular flux has the following form:

$$\psi(10, \mu) = e^{-\sigma_a(10\mu + \sqrt{11^2 - 10^2(1-\mu^2)})}, \quad \mu < 0, \quad (174)$$

where $\sigma_a = 2$ and $\sigma_a = 4$ for Problem 3 and Problem 3', respectively.

The solution in the central domain is constant and equals the value of the scalar flux resulting from the asymptotic diffusion boundary condition at $r=10$ formed by the anisotropic angular flux (Eq. (174)) entering from the pure absorbing subregion.

Figures 6 through 9 contain the results of this test problem. Figure 6 shows that both methods yield the same attenuated flux shape in the absorbing region. In Figure 7, we see that in the inner diffusive region, the methods have significant differences. The analytic result for the spatially constant flux in the inner region is 0.14674 found using Eq. (174) for $\sigma_a = 2$. The LCMOT solution is most accurate (1.1% relative error), and the SCMOT and MOT-SS solutions have a relative error of 11.2%. The MOT-LS solution shows that there is an increased error with a boundary condition present.

A second version of this problem (Problem 3'), defined in Table 5, is solved where the purely absorbing outer region has a larger total cross-section ($\sigma_t = \sigma_a = 4$). In this case, the analytic solution of the diffusion problem with the asymptotic boundary condition in the inner region has the value of 0.013989, found using

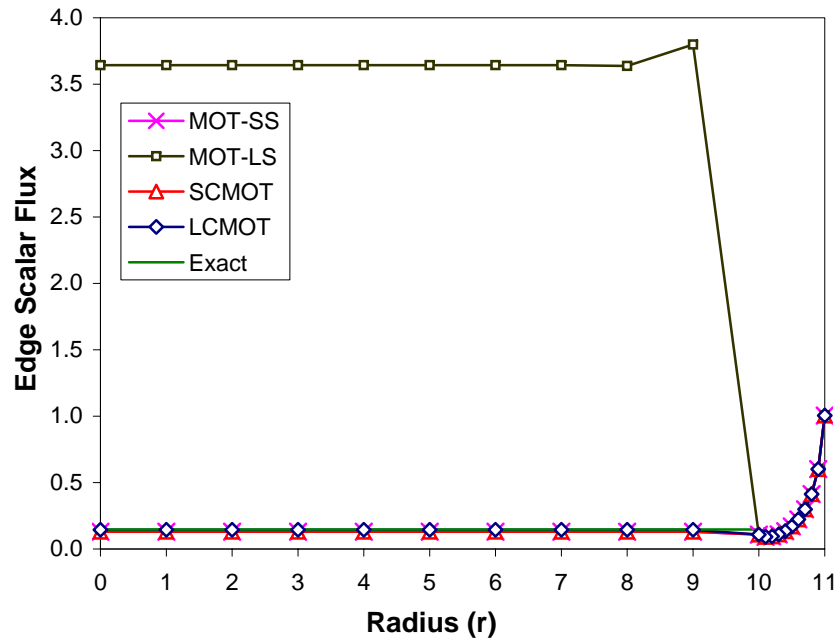


Figure 6: Problem 3 Solutions for all MOT Schemes.

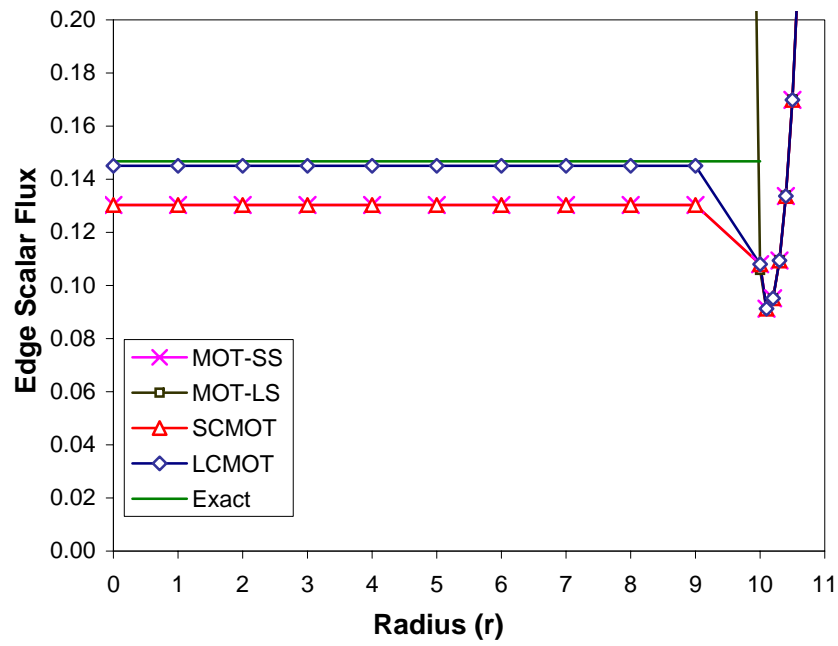


Figure 7: Problem 3 Interior Solutions for all MOT Schemes.

Eq. (174) for $\sigma_a = 4$. Figures 8 and 9 show that the relative error in the SCMOT and MOT-SS is about 14.2% with the relative error for LCMOT being about 0.5%.

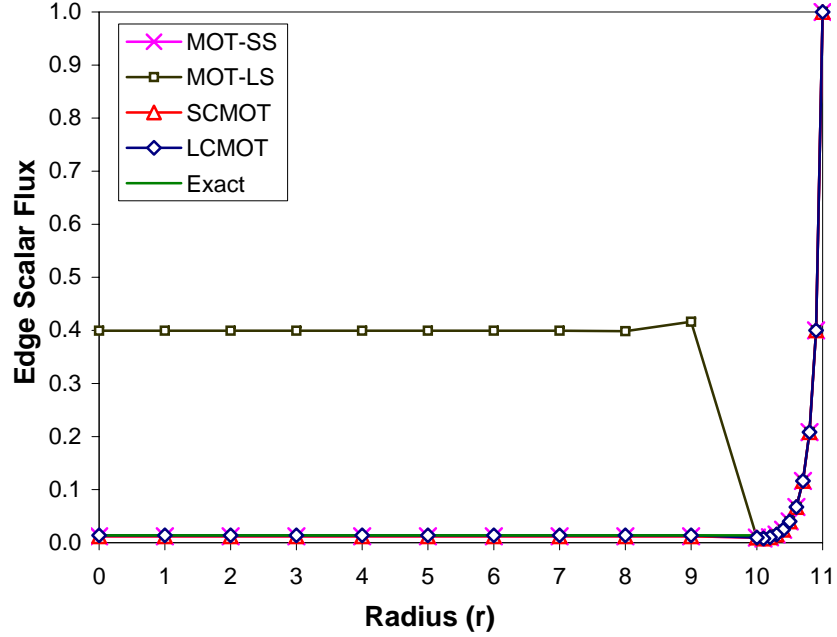


Figure 8: Problem 3' Solutions for all MOT Schemes.

Making use of the DSA scheme derived for LCMOT demonstrates how much faster the solutions can be obtained. Table 6 shows the differences in both the spectral radius and the number of iterations required to converge the solution.

Problem	Iterations	
	w/o DSA	w/ DSA
3	3722204	8
3'	3886290	8

Table 6: SI vs. DSA for LCMOT

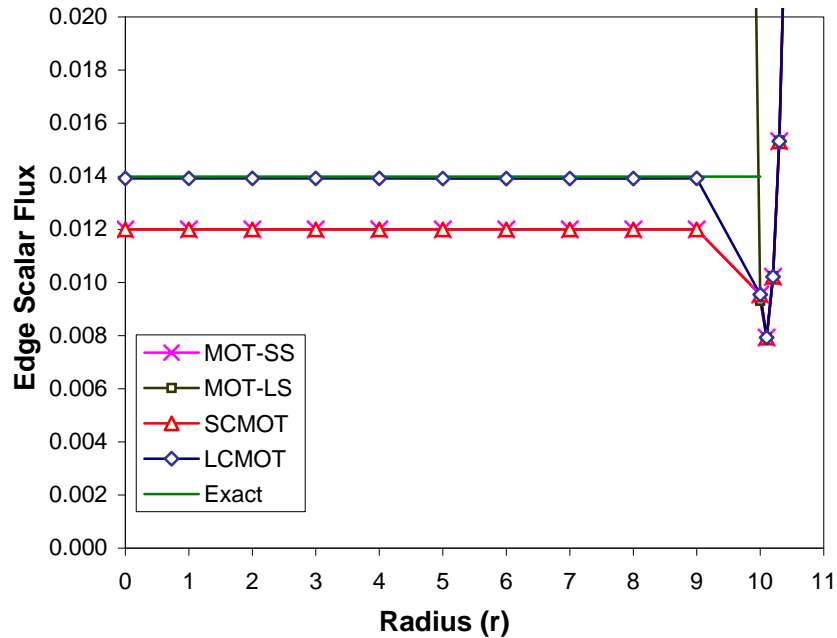


Figure 9: Problem 3' Interior Solutions for all MOT Schemes.

6.2.4 A Set of Tests on the Asymptotic Diffusion Limit

In this test problem, we consider a sequence of homogeneous spheres ($R = 10$) with $\sigma_t = \frac{1}{\varepsilon}$, $\sigma_a = \varepsilon$, and $q = \varepsilon$ [Ada 98], with a vacuum outer boundary. We solve each problem with a spatial mesh consisting of 10 uniform intervals.

Figure 10 shows the scalar flux obtained from the MOT-SS for various values of ε . As the value of ε in these tests decreases, the problem becomes more and more diffusive. It is clear from these figures that the solutions from the MOT-SS method are approaching zero, as predicted by our asymptotic analysis. This is completely unphysical, and is strong evidence that this method does not lead to a good approximation of the diffusion equation in the asymptotic diffusion limit.

Figure 11, however, shows that the original linear characteristic version, MOT-LS, approaches the solution of the diffusion equation for this problem. As ε ap-

proaches zero, the scalar flux solution in the problem interior becomes the infinite medium solution ($\phi = 1$) and the scalar flux on the boundary will be zero. Note that the the MOT-LS method is well behaved but this set of problems involves a vacuum boundary condition. An anisotropic incident angular flux boundary condition would likely cause the MOT-LS solutions to become much more inaccurate.

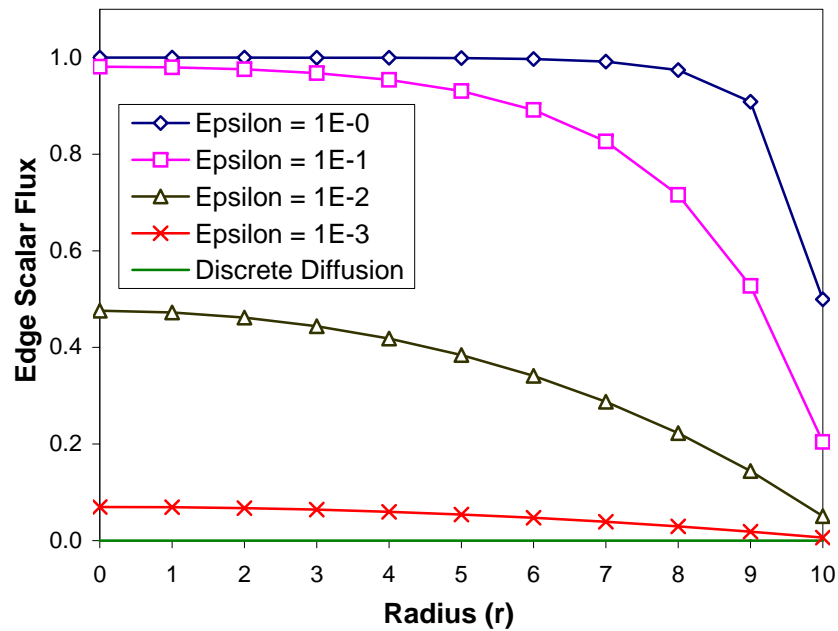


Figure 10: Problem 4 Solutions for the MOT-SS Scheme.

Figure 12 shows the scalar flux obtained from the SCMOT for various values of ε . The results shown are clearly the same as the results presented for the MOT-SS, and the same conclusions can be drawn.

Figure 13, however, shows that our new linear characteristic version of the MOT approaches the solution of the diffusion equation for this problem. As ε approaches zero, the scalar flux solution in the problem interior becomes the infinite medium solution ($\phi = 1$) and the scalar flux on the boundary will be zero.

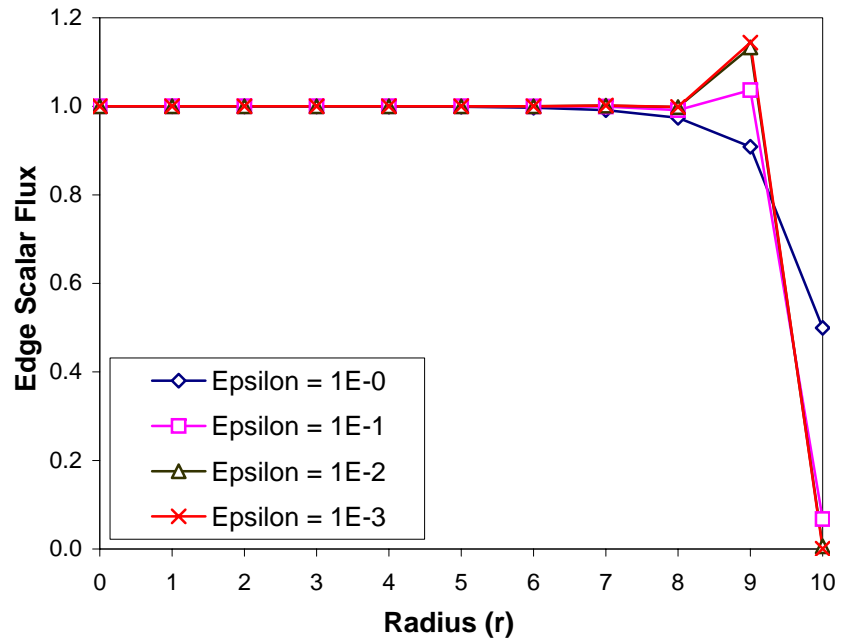


Figure 11: Problem 4 Solutions for the MOT-LS Scheme.

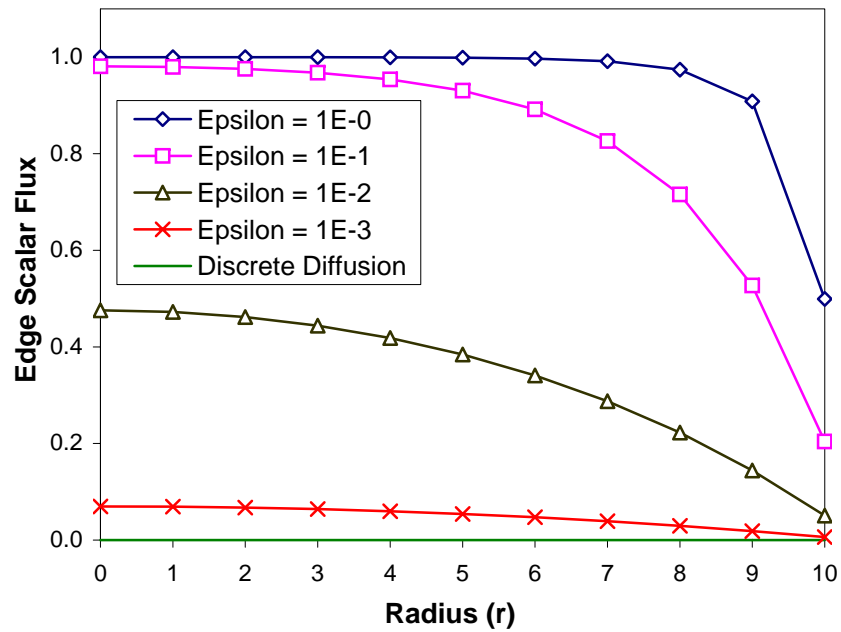


Figure 12: Problem 4 Solutions for the SCMOT Scheme.

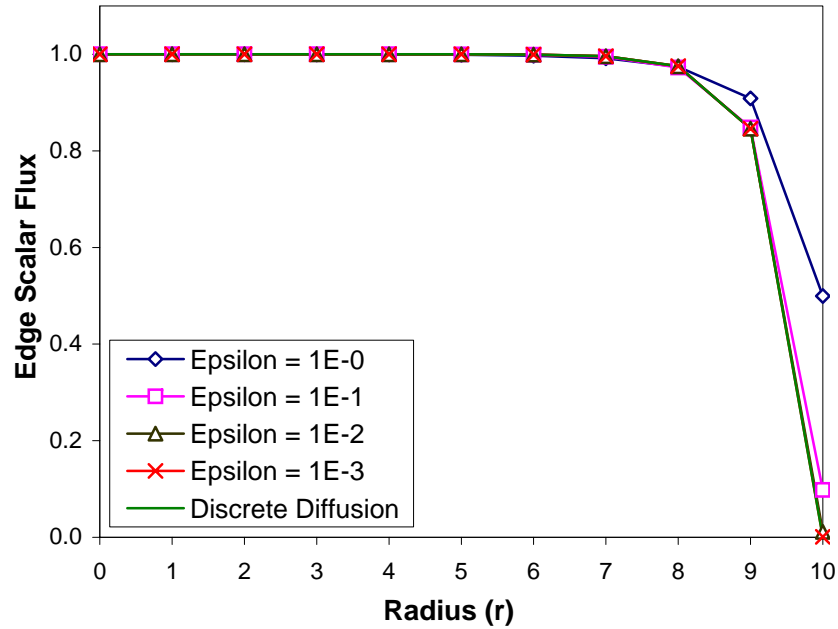


Figure 13: Problem 4 Solutions for the LCMOT Scheme.

To ensure that our code is working properly for both the LCMOT and the DSA schemes we plot the L_2 norm of the difference between the numerical result and the discrete diffusion solution, as ε approaches zero. Figure 14 demonstrates that the order of the error in the numerical results decreases linearly as ε decreases. Note that the solutions presented in Figure 14 were produced using the DSA scheme that has been developed.

Now that we have implemented the DSA scheme, we have the luxury of running this problem for smaller values of ε . Notice that the LCMOT scheme takes between 10^6 - 10^7 source iterations to converge for $\varepsilon = 10^{-3}$. The time and number of iterations to converge is prohibitively computationally expensive. Table 7 compares the accelerated method against the unaccelerated method and demonstrates the importance of accelerating the standard source iteration technique.

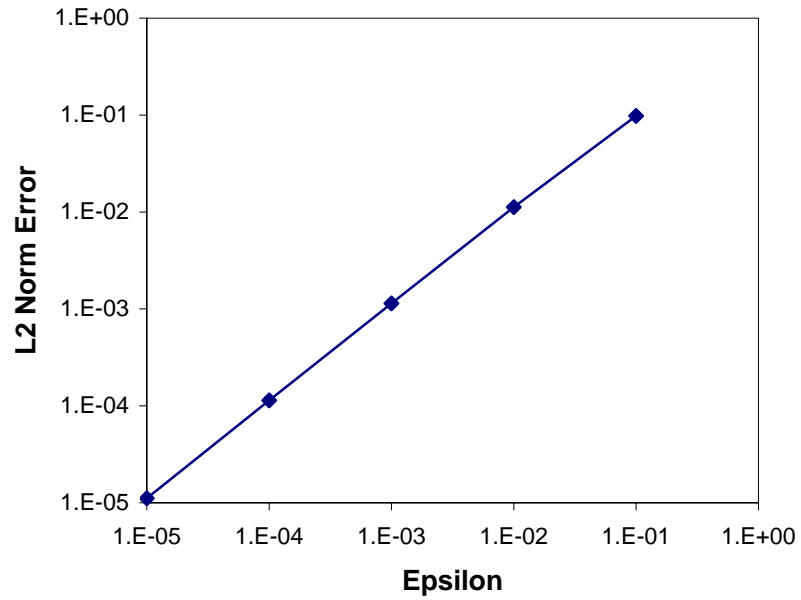


Figure 14: Problem 4 Error vs. Epsilon for the LCMOT Scheme.

Epsilon	Iterations	
	w/o DSA	w/ DSA
1E-1	988	7
1E-2	99175	6
1E-3	7496336	7
1E-4	n/a	7
1E-5	n/a	7

Table 7: SI vs. DSA for LCMOT

7 CONCLUSIONS

7.1 Introduction

In this chapter, we discuss the results of the research described in this thesis. In particular, the behavior of the original MOT discretizations and the moment-based MOT discretizations are analyzed. Also, the implementation of the DSA scheme for the linear moment-based method (LCMOT) is discussed. Some overall conclusions, as well as some recommendations for further research on MOT transport are given.

After implementing and analyzing the four MOT characteristic schemes we have drawn some generalized conclusions about the MOT. The MOT transport methods are different from those commonly in use today in several important ways:

- It is not an S_N method in the sense that the grid imposed on the angular variable μ is completely determined by the grid imposed on the spatial variable r .
- The transformation to the characteristic form eliminates the angular derivative in the spherical geometry transport equation. As a result, no differencing of this term is required. This is true for all members of the MOT family based on the original work by Nikiforova et al [Nik 72].
- The total number of cell-average angular flux unknowns required by the step and linear versions of the MOT are $N_r(N_r + 1)$ and $2N_r(N_r + 1)$, respectively, where N_r is the number of cells in the radial dimension. This is compared with WDD in angle/WDD in space $((N_\mu + 2)N_r)$, and WDD in angle/linear discontinuous finite element method in space $(2(N_\mu + 2)N_r)$,

where N_μ is the number of angles in the quadrature set. In general, for a given choice of spatial mesh, there will be more computational effort required

7.2 Original MOT Discretizations (MOT-SS and MOT-LS)

We have implemented two previously published spherical geometry methods and tested them in optically thick and diffusive regions. These methods make use of the angular integrated balance equation, and in the MOT-LS method, an approximate slope of the scalar flux. It has been shown that both methods perform poorly in optically thick and diffusive problems.

The original step method (MOT-SS) is identical to the moment-based step method (SCMOT). Therefore, given the results of the asymptotic analysis, the transport solution in the interior of a diffusive region satisfies discrete difference equations with no cross-section, grid thickness or source information. This result is unphysical in thick diffusive regions. This is made very clear in test Problem 4, where as ε tends toward zero, so does the solution. The MOT-SS method does not satisfy a proper diffusion discretization.

The transport solution observations in the interior of a diffusive region satisfies a reasonable approximation of the diffusion equation. However, the boundary condition observed can lead to very inaccurate solutions for optically thick and diffusive problems. This has been demonstrated in test Problems 3 and 3', where given an incident angular flux, the interior solution is orders of magnitude away from the exact interior solution. For the problems with a vacuum incident boundary condition (test Problems 1, 2 and 4), the solution on the interior is moderately well-behaved and accurate.

7.3 Moment-Based MOT Discretizations (SCMOT and LCMOT)

We have derived two new variants of the spherical geometry method of tubes in optically thick and diffusive regions. These new methods employ moments of the transport equation over the transformed coordinate system to represent the spatial shape of the scattering source.

Our asymptotic analysis, confirmed by numerical experiment, shows that both the step and linear MOT behave in a way that is analogous to their slab-geometry counterparts in optically thick and diffusive regions. The SCMOT transport solution in the interior of a diffusive region satisfies discrete difference equations with no cross-section, grid thickness or source information; as a result it is unphysical in thick diffusive regions. The LCMOT transport solution, however, satisfies a reasonable discretization of the diffusion equation with boundary conditions which are accurate approximations of those obtained in the analysis of the analytic spherical geometry transport equation.

While most of our numerical results were generated with standard source iteration with false convergence protection, we did employ a working diffusion synthetic acceleration for the LCMOT based on a linear discontinuous finite element diffusion equation. The use of a finite element diffusion equation to accelerate the convergence of characteristics methods was first demonstrated by Adams et al [Ada 98].

Though we haven't observed this behavior in the test problems we have included here, the three-point removal term in the discrete diffusion equation which is satisfied by the LCMOT has the potential to introduce unphysical oscillations in the scalar flux. This can be alleviated by "lumping" the first moment equation using a procedure developed in the finite element literature [Pal 93]. This will reduce the accuracy of the characteristic method, but will increase its robustness in

thick diffusive regions.

7.4 Diffusion Synthetic Acceleration of LCMOT

Last, we have derived a DSA scheme that can be applied to both an LDMOT and an LCMOT discretization. We have shown that the DSA scheme has significantly accelerated the convergence of the LCMOT method: with acceleration, our test problems converged in less than 10 iterations. This acceleration technique made it possible to easily solve test problems that are in the optically thick and diffusive regime.

By using the DSA scheme, we calculated the values presented in Fig. 14. We notice that the difference between transport and diffusion decreases linearly as the ε decreases. This is true because we are comparing against the leading order result of the asymptotic analysis. If we were to determine the asymptotic analysis solution to higher order, say $O(\varepsilon^2)$, the rate of convergence would be quadratic.

Of course, there may be difficulty in achieving this acceleration in multiple dimensions, but the value in 1-D transport is very clear.

7.5 Overall Conclusions and Future Work

We have analyzed two previously published MOT methods and two new MOT methods in optically thick and diffusive regions. The two methods previously published and the constant source moment-based method fail either in the interior of the problem or on the boundary. The linear source moment-based method limits to a reasonable discretization of the diffusion equation with accurate boundary conditions and an acceleration technique borrowed from the finite element literature has enhanced the capabilities of the method.

We plan to analyze and implement linear discontinuous finite element discretizations in this transformed one-dimensional spherical geometry coordinate system, where we can utilize the acceleration scheme developed in this thesis. We believe that it is possible to take any slab geometry discretization and develop an analogous 1-D spherical geometry discretization which will then have analogous properties (i.e. asymptotic diffusion limits, etc.) as the slab geometry method. In this respect, there is much work that can be done in this transformed coordinate system due to the volume of work previously performed in slab geometry.

Lastly, much like the work performed here in spherical geometry, a method for transforming a more general-geometry streaming operator into a slab-geometry-like streaming operator has been recently published [Tro 04]. In the future, we can make use of these procedures to develop the analogous characteristic schemes or finite element methods in these geometries. Also, asymptotic analyses can be completed to determine the validity of these methods in optically thick and diffusive regions.

BIBLIOGRAPHY

- [Ada 98] M.L. Adams, T.A. Wareing, and W.F. Walters, "Characteristic Methods in Thick Diffusive Problems," *Nucl. Sci. Eng.*, **130**, 18 (1998).
- [Ada 02] M.L. Adams and E.W. Larsen, "Fast Iterative Methods for Discrete-Ordinates Particle Transport Calculations," *Progress in Nuclear Energy*, **40**, 3 (2002).
- [Ani 08] D.Y. Anistratov and J. T. Fleming, "Asymptotic Diffusion Analysis of Conservative Methods of Long and Short Characteristics for 1D Spherical Geometry," *Trans. Am. Nucl. Soc.*, **98** (2008) (to appear).
- [Ask 72] J.R. Askew, "A Characteristic Formulation of the Neutron Transport Equation in Complicated Geometries," Atomic Energy Establishment, Winfrith Report M1108 (1972).
- [Cha 60] S. Chandrasekhar S., **Radiative Transfer**, Dover, New York (1960).
- [Lar 82] E.W. Larsen, "Unconditionally Stable Diffusion Synthetic Acceleration Methods for the Slab Geometry Discrete-Ordinates Equations. Part I: Theory," *Nucl. Sci. Eng.*, **82**, 47 (1982).
- [Lar 86] E.W. Larsen, J.E. Morel and W.F. Miller, Jr., "Asymptotic Solutions of Numerical Transport Problems in Optically Thick, Diffusive Regimes," *J. Comp. Physics*, **69**, 283 (1986).
- [Lar 90] E.W. Larsen and J.E. Morel, "Asymptotic Solutions of Numerical Transport Problems in Optically Thick, Diffusive Regimes II," *J. Comp. Physics*, **83**, 212 (1990).
- [Mor 84] J.E. Morel and G.R. Montry, "Analysis and Elimination of the Discrete-Ordinates Flux Dip," *Trans. Theory and Stat. Phys.* **13**, 615 (1984).
- [Nik 72] A.V. Nikofova, V.A. Tarasov and V.E. Troshchiev "Solution of the Kinetic Equations by the Divergent Method of Characteristics," *USSR Comp. Math. and Math. Phys.* **12**, 251-260 (1972)
- [Pal 91] T.S. Palmer and M.L. Adams, "Analysis of Spherical Geometry Finite Element Transport Solutions in the Thick Diffusion Limit," *Proc. of the International Topical Meeting of the American Nuclear Society—Advances in Mathematics, Computations, and Reactor Physics*, Vol. 5, p. 21.1 4-1 to 21.1 4-11, Pittsburgh, PA (1991).
- [Pal 93] T.S. Palmer, "Curvilinear Geometry Transport Discretizations in Thick Diffusive Regions," Ph.D. dissertation, University of Michigan. (1993).

- [Ree 71] W.H. Reed, "The Effectiveness of Acceleration Techniques for Iterative Methods in Transport Theory," *Nucl. Sci. Eng.*, **45**, 245 (1971).
- [Ris 08] M. E. Rising and T.S. Palmer, "An Analysis of the 1-D Spherical Geometry Method of Tubes in the Thick Diffusive Limit," *Trans. Am. Nucl. Soc.*, **98** (2008) (to appear).
- [Smi 02] K.S. Smith and J. D. Rhodes, III, "Full-Core, 2-D, LWR Core Calculations with CASMO-4E," *Proc. of the Int. Conf. on the New Frontiers of Nuclear Technology: Reactor Physics, Safety and High-Performance Computing (PHYSOR2002)*, Seoul, S. Korea (2002).
- [Tro 04] V.E. Troshchiev, A.V. Nifanova and Yu.V. Troshchiev, "Characteristic Approach to the Approximation of Conservation Laws in Radiation Transfer Kinetic Equations," *Doklady Mathematics*, **69**, No. 1, 136-140 (2004).
- [Vla 58] Vladimirov V.S., "Numerical solution of the Kinetic Equation for a Sphere," *Comp. Math.*, No. 3, 3-33(1958) (in Russian).
- [War 92] T. A. Wareing, "Asymptotic Diffusion Accelerated Discontinuous Finite Element Methods for Transport Problems," Ph.D. dissertation, University of Michigan. (1992).
- [War 07] J. S. Warsa and J. E. Morel, "Solution Algorithms for a P_{N-1} - Equivalent S_N Angular Discretization of the Transport Equation in One-dimensional Spherical Coordinates," *Proc. of the Joint International Topical Meeting on Mathematics and Computations and Supercomputing in Nuclear Applications, M&C + SNA 2007*, Monterey, CA (2007).